Equatorial Ocean Response to Rapidly Translating Wind Bursts

CHARLES C. ERIKSEN

School of Oceanography, University of Washington, Seattle, Washington

(Manuscript received 26 December 1991, in final form 17 August 1992)

ABSTRACT

The response of the ocean at low latitude to idealized westerly wind bursts can be described as a wave wake composed of equatorial gravity and Rossby–gravity modes. The excited waves are those with phase speeds that match the zonal translation speed of a wind burst, typically 10 m s^{-1}. These modes sum to produce oscillations near the local inertial frequency at each latitude, analogous to near-inertial internal gravity waves generated by moving storms at midlatitude. Linear theory predicts that typical wind burst amplitudes (stresses of 0.1 Pa) will generate substantial current oscillations [O (1 m s^{-1})] in the upper ocean. Response is initially confined to the region directly beneath a wind burst, after which the wake descends and refracts equatorward as a propagating beam. Waves are of sufficient amplitude to dominate shear and vertical strain in the upper ocean. Phase differences between oscillations at neighboring latitudes induce motion in the meridional–vertical plane at ever-decreasing meridional scales. Mixing associated with predicted low Richardson numbers is expected to check development of nonlinearity from vertical and meridional advection by the waves.

1. Introduction

While air–sea interaction in the tropics occurs on a variety of time and space scales, most recent research has emphasized mainly long-period, large-scale variability because of widespread interest in El Niño–Southern Oscillation phenomena and the seasonal cycle. Yet, evolution of upper-ocean structure on long time scales is often the result of a sequence of intense events. For example, seasonal deepening of the surface mixed layer at midlatitudes is accomplished via storms, which are relatively easily identified as discrete episodes. Recent investigations in the tropical western Pacific Ocean indicate that stratification of the tropical upper ocean depends in part on the occurrence of intense wind events anomalous to the seasonal cycle of gentle trade winds. Lukas and Lindstrom (1991) found that while a warm, rain-freshened surface layer usually caps the ocean in this region, occasional episodes of gale winds tend to mix the ocean well into the pycnocline. These mixing events have the effect of exposing the atmosphere to relatively cool water; hence, influencing air–sea fluxes of heat and moisture, and thus the sites and intensity of atmospheric convection. These wind events are commonly termed "westerly wind bursts" and the dynamical response of the ocean to these events is the subject of study reported here.

Westerly wind bursts were identified in Pacific island weather records by Luther et al. (1983) as episodes of relaxed trade winds lasting from a few days to a couple of weeks. In strong episodes, winds run counter to and are of comparable intensity to the trade winds normally found in the region. They occur most frequently from November through January and in El Niño years. The transition from easterlies (trades) to westerlies often takes place in only a few hours. These bursts are associated with disturbances in tropospheric circulation that meteorologists call "intraseasonal oscillations" or "30 to 60-day waves." Nakazawa (1988) demonstrates that cloud superclusters that are manifestations of intraseasonal oscillations carry behind them anomalous westerly winds, particularly evident between the Indonesian archipelago and the international date line.

A particular westerly wind burst seems even to have played a role in the course of history. While the occurrence of sudden westerly wind events was doubtless recognized by all who plied the tropical western Pacific for trade and conquest, an early report of the phenomenon comes in the account of Sir Francis Drake's circumnavigation during the reign of Queen Elizabeth of England. While sailing before northeast trade winds through the uncharted waters of the Celebes, Drake's ship foundered on a reef. His crew discarded several tons of loot and munitions, including cloves and cannons, in a vain attempt to free the ship, which was pressed upon the reef for almost a day by the trades. On the afternoon of 10 January 1580, the wind suddenly weakened, reversed direction, and freshened to a gale, driving the *Golden Hind* off the reef (Drake 1628; Wilson 1977; Lessa 1984; Sugden 1990). Drake then completed his voyage, surviving to later ravage the Spanish Main, defeat the Spanish Armada, and lay

Corresponding author address: Dr. Charles C. Eriksen, School of Oceanography WB-10, University of Washington, Seattle, WA 98195-0000.

the groundwork for England to build an empire through maritime conquest. While observational evidence is admittedly thin, the winds that saved Drake and his crew fit the general character of a westerly burst and occurred at the right time of year, although apparently not in an El Niño year. [Quinn et al. (1987) list 1578 as a very strong El Niño year, making westerly bursts likely late that year and early in 1579.]

The characteristic space–time structure of westerly wind bursts determines what motions are excited by these bursts in the tropical ocean. Island wind records indicate that westerly bursts have long zonal and narrow meridional extent. They can be described reasonably well by a Gaussian shape in latitude, typically only a few degrees wide, and are most often centered on the equator or a few degrees south of it (Harrison and Giese 1991). They turn on and off over a day or two, last a few days to a week or two, are manifested in mainly zonal winds, and attain westerly wind speeds of 8–12 m s^{-1} at the ocean surface. Nakazawa (1988) demonstrated the link between intraseasonal oscillations, which take the form of eastward-propagating (global) wavenumber one waves of one or two-month period, and westerly wind disturbances following cloud superclusters. These eastward-traveling cloud superclusters are fed by convergent motion in the lower troposphere; hence westerly winds follow the clouds and are particularly intense in the western Pacific over a large pool of very high sea surface temperatures (leading to annual rainfall as high as 5 m). The cases Nakazawa presented indicate that westerly wind bursts propagate eastward at roughly 10 m s^{-1} with zonal scales of 1000 km or so.

The response of the tropical ocean to idealized westerly wind bursts with the characteristics described above is considered in this paper. Because they translate zonally at speeds faster than the phase speed of the gravest internal-mode Kelvin wave in the ocean, westerly wind bursts are particularly effective in exciting equatorial gravity wave modes, much as a midlatitude storm excites slightly superinertial internal gravity waves (Kundu and Thompson 1985). That impulsively initiated winds excite gravity modes was noticed by Moore and Philander (1978), but they considered merely a single baroclinic mode in their tropical modeling review. While very many papers written following Lighthill (1969) describe models of low-latitude oceanic response to wind forcing, very few have bothered to include equatorial gravity wave modes in the solution. This is largely because interest has focused on low-frequency variability. Exceptions are Wunsch and Gill (1976) and Luther (1980), in which peaks in equatorial island sea level spectra are explained as being due to energy accumulating near frequencies corresponding to vanishing zonal group speed of equatorial gravity wave modes. In practice, these frequencies are indistinguishable from those of vanishing zonal wavenumber, hence infinite zonal phase speed. Wunsch and Gill offered a model of wave forcing by broadband wind stress fluctuations but concentrated only on sea level response. As the calculations presented here demonstrate, a rapidly translating wind burst of modest strength will generate robust current fluctuations as a gravity wave wake trailing behind it. This wake appears as a train of local slightly superinertial internal gravity waves at each latitude.

Recent attention to wind burst response in the western Pacific has centered on the generation of Kelvin waves. Wind systems that translate more slowly than the wave speeds of available Kelvin modes generate Kelvin and Rossby modes, as shown by McCreary and Lukas (1986). The analogous solution for a rapidly translating wind system is presented here, where gravity modes rather than Rossby modes are resonant. Giese and Harrison (1990, 1991) used a numerical model to calculate the response to a stationary wind patch with the spatial characteristics of a westerly burst. Not surprisingly, the solution was dominated by Kelvin wave generation. By contrast, the wave wake left by a rapidly translating wind burst includes a Kelvin mode only as a member of the directly forced equatorial (Yoshida) jet solution. Equatorial gravity waves are manifested as robust current fluctuations found not only within the jet, but at higher latitudes and deeper depths as well. Because the vertical shear produced by an equatorial gravity wave wake is both intense and meridionally widespread, these waves can be expected to be a principal source of upper-ocean mixing in the tropics.

The approach taken here is to calculate the linear response of a realistically stratified ocean to deterministic wind stress patterns that approximate westerly wind bursts. The model equations are developed in section 2, followed by a discussion of what wave modes are excited by wind bursts with different characteristics in section 3. The spatial and temporal structure of linear response to particular wind events is described in section 4 and the implications of the linear calculation for advection and mixing are discussed in sections 5 and 6. A discussion of the limitations of these calculations appears with conclusions in section 7.

2. Model of a continuously stratified equatorial ocean forced by wind stress

The features essential to wave response that distinguish the tropical ocean dynamically from other regions are its stratification, meridional variation of planetary vorticity, and mean current structure. The essential features that characterize westerly wind bursts are narrow meridional confinement and rapid eastward translation. Mean current structure can be neglected in wave response to rapidly translating forcing. The simplest model that retains the remaining features with some realism while remaining analytically tractable is one for a continuously stratified ocean where the back-

ground buoyancy frequency profile $N(z)$ is laterally invariant, consistent with a resting basic state, and variation of the Coriolis parameter f with latitude is modeled by an equatorial β plane, $f = \beta y$, where y is the northward coordinate. The ocean is taken to have constant depth d and be unbounded laterally. Wind stress is applied as an equivalent body force in the surface mixed layer. This stress divergence structure projects onto the dynamical modes of a flat-bottomed ocean and linear solutions are sought. This kind of model has been used frequently in equatorial oceanography, although even for modest forcing amplitudes, nonlinear advection of momentum and density can be significant. Nonlinearities notwithstanding, a model for linear response to a wind stress pattern translating at a fixed zonal speed U is developed in this section.

The Boussinesq hydrostatic equations for momentum conservation and the equation for mass conservation for this simple system are

$$u_t - fv = -p_x + H(z+h)\tau^x/h \quad (1a)$$

$$v_t + fu = -p_y + H(z+h)\tau^y/h \quad (1b)$$

$$p_{zt} + N^2 w = 0 \quad (1c)$$

$$u_x + v_y + w_z = 0, \quad (1d)$$

where u, v, and w are the perturbation current components in the eastward, northward, and upward directions, respectively; p is reduced perturbation pressure; H is the Heaviside step function; τ^x and τ^y are the zonal and meridional components of normalized surface wind stress (stress divided by reference density ρ_0); $N(z) \equiv (-g\rho_{1z}(z)/\rho_0)^{1/2}$ is the buoyancy frequency of the resting ocean; and $\rho_0 + \rho_1(z)$ is its resting density ($\rho_1 \ll \rho_0$). Independent variables as subscripts denote derivatives and h is the depth of the surface mixed layer over which wind stress is applied. The system (1) is subject to free surface and flat bottom boundary conditions so that current and pressure can be projected onto baroclinic modes as

$$u(x, y, z, t) = \sum_m u_m(x, y, t) \cdot G'_m(z) \quad (2a)$$

$$v(x, y, z, t) = \sum_m v_m(x, y, t) \cdot G'_m(z) \quad (2b)$$

$$p(x, y, z, t) = \sum_m p_m(x, y, t) \cdot G'_m(z) c_m \quad (2c)$$

$$w(x, y, z, t) = \sum_m p_{mt}(x, y, t) \cdot G_m(z)/c_m. \quad (2d)$$

Then the system of three equations describing motion in each vertical mode m takes the form of that for an equivalent shallow-water barotropic system of depth c_m^2/g:

$$u_{mt} - fv_m + c_m p_{mx} = \tau^x_m \quad (3a)$$

$$v_{mt} + fu_m + c_m p_{my} = \tau^y_m \quad (3b)$$

$$u_{mx} + v_{my} + p_{mt}/c_m = 0, \quad (3c)$$

where $G_m(z)$ satisfies the vertical structure equation $G''_m + (N(z)/c_m)^2 G_m = 0$ subject to the normalization $\int_{-d}^{0} G'_m(z)^2 dz = d$, c_m is the eigenspeed of the mth vertical mode, and the coupling coefficients are defined by $\tau^x_m \equiv \tau^x G'_m(0)/d$ and $\tau^y_m \equiv \tau^y G'_m(0)/d$. For forcing that translates zonally at a speed U, the time derivative operator ∂_t is equivalent to $-U \cdot \partial_x$ so that a governing equation for meridional velocity involving only spatial derivatives can be found from (3):

$$(U^2/c_m^2 - 1)v_{mxx} - v_{myy} + [(\beta y/c_m)^2 + \beta/U]v_m = U^{-1}(\tau^y_{mx} - \tau^x_{my}) - \beta y c_m^{-2}\tau^x_m - (U/c_m^2)\tau^y_{mx}. \quad (4)$$

Meridional current for each vertical mode $v_m(x, y)$ may be projected onto Hermite functions $\psi_n(\eta) = (2^n n!\sqrt{\pi})^{-1/2} \exp(-\eta^2/2) H_n(\eta)$; the normal modes on an equatorial β plane, as

$$v_m(x, y) = \sum_n q_{mn}(x)\psi_n(\eta), \quad (5)$$

where $\eta = y(\beta/c_m)^{1/2}$ is the meridional coordinate scaled by the equatorial deformation radius and $H_n(\eta)$ are the Hermite polynomials. Then the governing equation (4) becomes an ordinary differential equation for the amplitude $q_{mn}(x)$ of vertical mode m and meridional mode n:

$$q_{mnxx} + k_{mn}^2 q_{mn} = -U^{-1}\int_{-\infty}^{\infty} \tau^y_{mx}\psi_n d\eta - (U^2 - c_m^2)^{-1} \times \{c_m^2 U^{-1}(\beta/c_m)^{1/2}\int_{-\infty}^{\infty} \tau^x_{m\eta}\psi_n d\eta + (\beta c_m)^{1/2}\int_{-\infty}^{\infty} \tau^x_m \eta \psi_n d\eta\}. \quad (6)$$

This equation indicates that meridional current fluctuations are forced by the two wind stress components through different projections on their spatial structure. These amount to different responses to stress curl and Ekman transport divergence.

To evaluate the integrals describing forcing in (6), particular forms for wind stress components must be chosen. A reasonable idealization of westerly wind burst structure is a boxcar in longitude times a Gaussian in latitude centered at $y = y_0$ with a meridional width L. That is, the model burst arrives suddenly, maintains a constant strength, and then suddenly departs, as observations suggest. The boxcar in longitude can be constructed as the sum of two step functions that are equal and opposite but lagged spatially. When $\tau(x, y) = \tau_0(1 - H(x)) \exp\{-[(y - y_0)/L]^2\}$ where $H(x)$ is the Heaviside step function, the solution to (6) is a sum of Hermite functions modulated by sines and cosines behind the front ($x \leq 0$) for wind patterns that

translate at speeds faster than the Kelvin wave speed for each baroclinic mode ($U > c_m$). The solution vanishes ahead of the jump in stress. For slow moving wind patterns ($U < c_m$), the solution decays exponentially (evanescent waves) both ahead of and behind the jump. Expressions for meridional current $v(x, y, z)$ for the two cases are

$$U > c_m, \quad x \leq 0: v(x,y,z) = \sum_m G'_m(z) \sum_n \psi_n(\eta) \cdot \{-\tau^y_m (k_{mn}U)^{-1} A_{mn} \sin(k_{mn}x) + \tau^x_m [(U^2 - c_m^2)k_{mn}^2]^{-1} (\beta c_m)^{1/2} [B_{mn} + (c_m/U)C_{mn}][\cos(k_{mn}x) - 1]\}, \quad (7a)$$

$$U > c_m, \quad x \geq 0: v(x,y,z) = 0, \quad (7b)$$

$$U < c_m, \quad x \leq 0: v(x,y,z) = \sum_m G'_m(z) \sum_n \psi_n(\eta) \cdot \{-\tau^y_m (k_{mn}U)^{-1} A_{mn} \exp(k_{mn}x) + \tau^x_m [(U^2 - c_m^2)k_{mn}^2]^{-1} (\beta c_m)^{1/2} [B_{mn} + (c_m/U)C_{mn}][2 - \exp(k_{mn}x)]\}/2, \quad (7c)$$

$$U < c_m, \quad x \geq 0: v(x,y,z) = \sum_m G'_m(z) \sum_n \psi_n(\eta) \cdot \{-\tau^y_m (k_{mn}U)^{-1} A_{mn} \exp(-k_{mn}x) + \tau^x_m [(U^2 - c_m^2)k_{mn}^2]^{-1} (\beta c_m)^{1/2} [B_{mn} + (c_m/U)C_{mn}][\exp(-k_{mn}x)]\}/2, \quad (7d)$$

where zonal wavenumber is given by

$$k_{mn} = \{\beta c_m (2n + 1 + c_m/U)/|U^2 - c_m^2|\}^{1/2}. \quad (8)$$

The constants A_{mn}, B_{mn}, and C_{mn} are meridional integrals of the wind stress structure defined by

$$A_{mn} = \int_{-\infty}^{\infty} \psi_n(\eta) \exp\{-[(y - y_0)/L]^2\} d\eta \quad (9a)$$

$$B_{mn} = \int_{-\infty}^{\infty} \psi_n(\eta)\eta \exp\{-[(y - y_0)/L]^2\} d\eta \quad (9b)$$

$$C_{mn} = \int_{-\infty}^{\infty} \psi_n(\eta)\partial_\eta[\exp\{-[(y - y_0)/L]^2\}] d\eta. \quad (9c)$$

These can be evaluated using the rules for projection on Hermite functions (McCreary 1980), derived using recursion relations for these functions. These state that, given A_{mn}, $B_{mn} = [(n+1)/2]^{1/2} A_{mn+1} + (n/2)^{1/2} A_{mn-1}$ and $C_{mn} = [(n+1)/2]^{1/2} A_{mn+1} - (n/2)^{1/2} A_{mn-1}$. Defining the parameters $a = c_m/(\beta L^2)$ and $b = y_0(\beta/c_m)^{1/2}$, A_{mn} can be found as

$$A_{mn} = [2\pi/(2a + 1)]^{1/2} \exp\{ab^2/(4a^2 - 1)\} \times [(2a - 1)/(2a + 1)]^{n/2} \psi_n\left[ab \Big/ \left(a^2 - \frac{1}{4}\right)^{1/2}\right] \quad (10)$$

(D. Moore 1991, personal communication. Also, $B_{m0} = C_{m0} = A_{m1}/\sqrt{2}$, $B_{m1} = A_{m2} + A_{m0}/\sqrt{2}$, and $C_{m1} = A_{m2} - A_{m0}/\sqrt{2}$.

Expressions for the zonal derivatives of zonal current and pressure can be found from (3). These are easily integrated zonally to obtain expressions for zonal current and pressure:

$$U > c_m, \quad x \leq 0: u(x,y,z) = \sum_m G'_m(z)[-\tau^x_m Ux/(U^2 - c_m^2) + (\beta c_m)^{1/2} \sum_n \theta_n(\eta) \times \{\tau^y_m (k_{mn}^2 U)^{-1} A_{mn}(\cos(k_{mn}x) - 1) + \tau^x_m [(U^2 - c_m^2)k_{mn}^3]^{-1} \times (\beta c_m)^{1/2} [B_{mn} + (c_m/U)C_{mn}][\sin(k_{mn}x) - k_{mn}x]\}], \quad (11a)$$

$$p(x,y,z) = \sum_m G'_m(z)[-\tau^x_m c_m^2 x/(U^2 - c_m^2) + c_m(\beta c_m)^{1/2} \sum_n \varphi_n(\eta) \times \{\tau^y_m (k_{mn}^2 U)^{-1} A_{mn}(\cos(k_{mn}x) - 1) + \tau^x_m [(U^2 - c_m^2)k_{mn}^3]^{-1} \times (\beta c_m)^{1/2} [B_{mn} + (c_m/U)C_{mn}][\sin(k_{mn}x) - k_{mn}x]\}], \quad (12a)$$

$$U > c_m, \quad x \geq 0: u(x,y,z) = 0 \quad (11b)$$

$$p(x,y,z) = 0 \quad (12b)$$

$$U < c_m, \quad x \leq 0: u(x,y,z) = \sum_m G'_m(z)[-\tau^x_m Ux/(U^2 - c_m^2) + (\beta c_m)^{1/2} \sum_n \theta_n(\eta) \times \{\tau^y_m (k_{mn}^2 U)^{-1} A_{mn}(2 - \exp(k_{mn}x)) + \tau^x_m [(U^2 - c_m^2)k_{mn}^3]^{-1} \times (\beta c_m)^{1/2} [B_{mn} + (c_m/U)C_{mn}][2k_{mn}x - \exp(k_{mn}x)]\}/2], \quad (11c)$$

$$p(x, y, z) = \sum_m G'_m(z)[-\tau^x_m c^2_m x/(U^2 - c^2_m) + c_m(\beta c_m)^{1/2} \sum_n \varphi_n(\eta)$$
$$\times \{\tau^y_m(k^2_{mn}U)^{-1}A_{mn}(2 - \exp(k_{mn}x)) + \tau^x_m[(U^2 - c^2_m)k^3_{mn}]^{-1}$$
$$\times (\beta c_m)^{1/2}[B_{mn} + (c_m/U)C_{mn}][2k_{mn}x - \exp(k_{mn}x)]\}/2], \quad (12c)$$

$U < c_m$, $x \geq 0$: $u(x, y, z) = \sum_m G'_m(z)[(\beta c_m)^{1/2} \sum_n \theta_n(\eta)$
$$\times \{\tau^y_m(k^2_{mn}U)^{-1}A_{mn}(\exp(-k_{mn}x)) + \tau^x_m[(U^2 - c^2_m)k^3_{mn}]^{-1}$$
$$\times (\beta c_m)^{1/2}[B_{mn} + (c_m/U)C_{mn}][\exp(-k_{mn}x)]\}/2], \quad (11d)$$

$$p(x, y, z) = \sum_m G'_m(z)[c_m(\beta c_m)^{1/2} \sum_n \varphi_n(\eta)$$
$$\times \{\tau^y_m(k^2_{mn}U)^{-1}A_{mn}(\exp(-k_{mn}x)) + \tau^x_m[(U^2 - c^2_m)k^3_{mn}]^{-1}$$
$$\times (\beta c_m)^{1/2}[B_{mn} + (c_m/U)C_{mn}]\exp(-k_{mn}x)\}/2]. \quad (12d)$$

The meridional structures of these quantities are specified through

$$\theta_n(\eta) = -(n/2)^{1/2}\psi_{n-1}(\eta)/(U + c_m) - [(n + 1)/2]^{1/2}\psi_{n+1}(\eta)/(U - c_m) \quad (13a)$$

$$\varphi_n(\eta) = (n/2)^{1/2}\psi_{n-1}(\eta)/(U + c_m) - [(n + 1)/2]^{1/2}\psi_{n+1}(\eta)/(U - c_m). \quad (13b)$$

Notice that two terms in each expression (11a,c), (12a,c) describe linear growth in x. This portion of the solution, commonly referred to as the equatorial or Yoshida jet, is confined to the region in depth over which wind stress is applied (here, the mixed layer $-h < z < 0$). Expressions for the spatial and temporal derivatives of current and pressure needed to evaluate other flow field variables are easily found from (7), (11), and (12).

Response to translating Gaussian wind patches of finite zonal extent can be described as the difference between the above solution and an identical one lagged by a prescribed zonal distance. While the solutions are analytic, the sums must in practice be performed numerically. Baroclinic mode shapes $G(z)$ were calculated from an average $N(z)$ profile based on conductivity–temperature–depth (CTD) casts collected in the western Pacific between 4°N and 4°S along 155°E by R. Lukas. The first 50 baroclinic modes were used in the above sums for this study. Except for calculations involving meridional derivatives of zonal current or pressure, solutions were evaluated by summing the analytic solutions for meridional modes n = 0–99. Sums over modes n = 0–199 were required in the exceptional cases to allow quantities found from differentiated fields to be comparably smooth to those not evaluated from derivatives. The number of meridional modes in the solution is determined from the requirement that the highest meridional mode of the slowest baroclinic mode have a turning latitude beyond the meridional domain considered. Solutions were evaluated in planes aligned normal to the vertical, zonal, and meridional directions using a grid of 41 × 151 = 6191 or 41 × 101 = 4141 points. The evaluations and summing of 10^4 modes to calculate 20 flow variable terms at each grid point required approximately one hour of computing time on a Sun Microsystems model Sparcstation1+ computer workstation.

3. Wave response spectra

The dispersion characteristics of equatorial waves are such that a rapidly traveling wind pattern will excite only gravity and Rossby–gravity modes. Rossby modes are at most one-third as fast as Kelvin modes and westward, but even the fastest Kelvin mode is slow compared to typical eastward translation speeds of westerly bursts. The dispersion curves based on western Pacific stratification are drawn in Fig. 1, along with a typical translation speed for a westerly burst, 10 m s^{-1}. The Kelvin, Rossby–gravity, and first meridional mode (n = 1) Rossby and gravity dispersion curves are given in this figure for the first 20 baroclinic modes. The intersections of these curves with the heavy line indicate the frequency–zonal wavenumber pairs of the equatorial waves excited by a translating wind pattern. While the highest-frequency such wave indicated in the figure has a period of just under five days, most of the wave modes excited have periods around 20 days. The pattern extends to higher frequencies for higher meridional modes without altering the basic result: response is dominated by high baroclinic mode waves at low frequencies because these modes are so densely spaced.

How effectively each vertical mode is excited depends on stratification. For comparison, mode shapes for buoyancy frequency profiles typical of the equatorial western Pacific are shown in Fig. 2 where the only difference between the profiles is the thickness of the mixed layer h. The left panel of this figure shows mode shapes based on the observed average buoyancy frequency at 155°E within 4° of the equator except

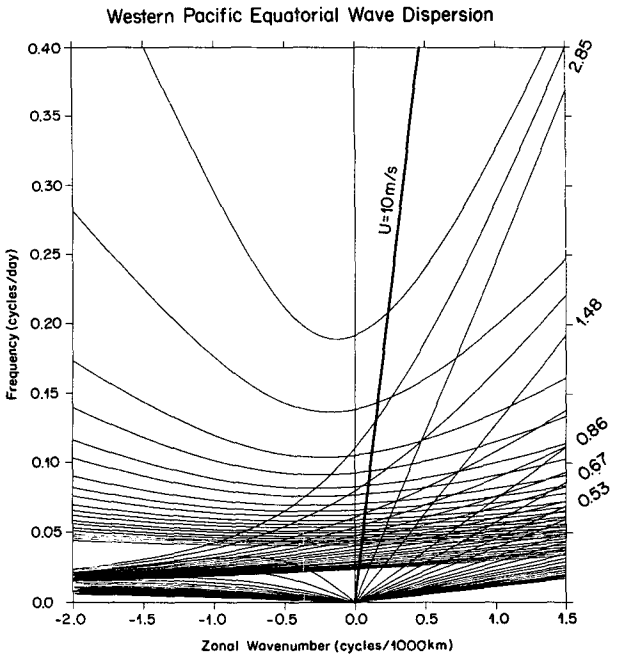

FIG. 1. Dispersion curves (thin curves) for free first meridional mode equatorial Rossby and gravity, Kelvin, and Rossby–gravity waves for the first 20 baroclinic modes based on stratification near 0°, 155°W. Intersections with the heavy line indicate frequencies and zonal wavenumbers of waves that will be excited by a wind burst traveling eastward at 10 m s^{-1}. Phase speeds of Kelvin waves of the first five vertical modes are indicated in meters per second.

that buoyancy frequency $N(z)$ has been set to zero for depths shallower than 30 m to include a surface mixed layer. The right panel shows the mode shapes for an identical $N(z)$ profile except that the mixed-layer depth has been set to $h = 100$ m. The mode shapes for the two profiles are similar for depths deeper than the pycnocline but differ substantially closer to the surface. In particular, when $h = 100$ m, the surface value $G'_m(0)$ of the mode shape describing horizontal current is much higher for the first baroclinic mode $m = 1$ than for higher modes. For a thinner mixed layer, $h = 30$ m, $G'_m(0)$ is somewhat higher for the fourth, fifth, and sixth modes than for modes other than the first. The relative contribution of each mode, $(h/d)G'_m(0)^2$, in describing the variance of the prescribed step function form of stress divergence is plotted in Fig. 3 for the two mixed-layer depth choices, where these terms sum to unity for an infinite number of modes. While modes $m = 3$–10 are similarly excited for the two mixed-layer depth choices, stress projects on a broader band of vertical modes and the first baroclinic mode is less prominent when the mixed layer is thinner.

The joint vertical wavenumber–frequency spectrum E_{mn} of wave response can be calculated as an integral over depth and latitude:

$$E_{mn} = \frac{\rho_0}{2}\int_{-\infty}^{\infty} dy \int_{-d}^{0} dz[u_{mn}^2 + v_{mn}^2 + (N(z)w_{mn}/\omega_{mn})^2], \quad (14)$$

where u_{mn}, v_{mn}, and w_{mn} refer to the oscillating portion of the zonal, meridional, and vertical current components for each vertical and meridional mode, and frequency $\omega_{mn} = k_{mn}U$ is determined through the dispersion relationship (8); E_{mn} describes the wave response kinetic plus potential energy per unit zonal distance in each mode to step function surface wind stress excitation specified by τ_0^x and τ_0^y. The integrals are easily evaluated through the vertical–meridional decomposition (2) and the solutions (7), (11), and (12) to produce an expression for the response spectrum:

$$E_{mn} = (\rho_0/4)G'_m(0)^2 d^{-1}(c_m/\beta)^{1/2}\{1 + [n/(U + c_m)^2 + (n + 1)/(U - c_m)^2](U^2 - c_m^2)/(2n + 1 + c_m/U)\} \times \{(\tau_0^y k_{mn}^{-1} U^{-1} A_{mn})^2 + (\tau_0^x[(U^2 - c_m^2)k_{mn}^2]^{-1}(\beta c_m)^{1/2}[B_{mn} + (c_m/U)C_{mn}])^2\}. \quad (16)$$

The wave energy in any particular vertical–meridional-mode pair depends on how effectively the forcing projects on that mode, both vertically [through $G'_m(0)$] and horizontally (through A_{mn}, B_{mn}, C_{mn}, and c_m/U). The total wave energy $E = \Sigma_m\Sigma_n E_{mn}$ is inversely proportional to mixed-layer depth h, since $\Sigma_m(h/d)G'_m(0)^2 = 1$.

How effectively each meridional mode is excited depends on the meridional scale of the wind stress pattern applied and the direction of the wind stress. Plots of the wave energy per unit zonal distance E_{mn} excited in the gravest 11 meridional modes and 100 vertical modes are shown in Fig. 4 for various wind stress patterns applied to a thin mixed layer ($h = 30$ m). All are Gaussians in latitude with width $L = 3.6°$ (as suggested by Harrison and Giese 1991), translate at $U = 10$ m s^{-1} (as suggested by Nakazawa 1988), and are single steps in longitude (i.e., wind turns on and stays on behind a translating front). The two upper panels in Fig. 4 are for a wind pattern centered on the equator ($y_0 = 0°$) while the lower panels have wind centered at 3° latitude ($y_0 = 3°$). The left two panels in this figure are for a stress jump of 0.1 Pa in zonal wind and the right two are for a jump of the same size in meridional wind. A comparison of the right two panels with the left two demonstrates that zonally translating changes in meridional stress excite the available equatorial wave modes more effectively than do equal changes in zonal stress. As expected from the structure of the solutions (7), (11), and (12), zonal stress applied with even symmetry about the equator excites only waves with

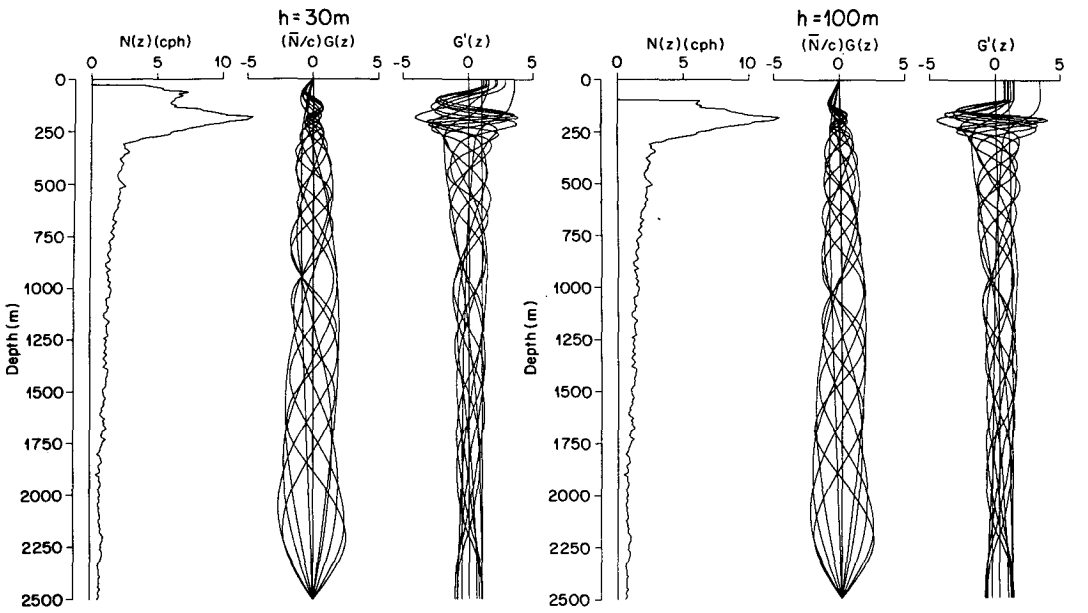

FIG. 2. Mode shapes for the barotropic and first ten baroclinic modes for surface mixed layers h = 30 m deep (left panel) and h = 100 m deep (right panel). Each panel shows profiles of buoyancy frequency $N(z)$ and mode shapes $G_m(z)$ and $G'_m(z)$ describing structure of vertical and horizontal motions, respectively. The stratification, based on CTD profiles from 4°N to 4°S along 155°W, is identical in the two cases except for the depth of the mixed layer, where $N(z)$ has been set to zero.

even symmetry in zonal current (i.e., n odd: top left panel) while a meridional stress with the same shape excites only waves with even symmetry in meridional current (i.e., n even: top right panel). Stress patterns centered off the equator excite all meridional modes (lower panels). As expected from the dispersion curves (Fig. 1), most energy is concentrated at periods 10 days and longer (higher vertical modes have longer periods to maintain the prescribed zonal phase speed of 10 m s^{-1}). The relative contributions of vertical modes indicated in Fig. 3 are distorted in Fig. 4, but still recognizable. In particular, baroclinic modes m = 4–6 tend to be the most energetic in each of these examples. The relative weakness of lower (higher) baroclinic modes compared to these is due to their broad (narrow) scale relative to that of the prescribed wind stress pattern.

Response is sensitive to mixed-layer thickness because stress applied at the ocean surface is converged uniformly and completely through the mixed layer in this model. Not only will the distribution of energy with vertical mode be narrower for a thicker mixed layer (as in Fig. 3), but the total response summed over all modes energy will diminish in inverse proportion to mixed-layer thickness, as discussed above. Comparison of spectra for h = 100 m (Fig. 5) with those for h = 30 m (Fig. 4), where the details of forcing are otherwise identical, demonstrates this result. In addition to having narrower bandwidth in vertical mode and smaller total response, excitation through a thicker mixed layer skews the response to a lower vertical mode number range, hence higher frequency. For example, excitation through a thicker mixed layer by a wind pattern centered off the equator is nearly the same in the lowest two vertical modes as when the mixed layer is thinner, but much smaller for higher vertical modes (compare the lower two panels of Fig. 5 with the same two panels in Fig. 4).

The duration of a wind burst affects the mixture of modes excited by interference of the wave wakes generated by the leading and trailing edges of the burst. The panels in Fig. 6 depict wave response to two equal but opposite step changes in wind separated in time by differing amounts. As these panels show, longer bursts tend to generate bigger wave wakes and waves at frequencies equal to integral numbers of cycles per burst length cancel. The fundamental frequency of a 10 d burst is 0.10 cycles per day (cpd); hence, the wave wake for this burst contains no energy at this frequency and its multiples (lower right panel, Fig. 6). The shorter bursts considered in the examples of Fig. 6 have fundamental frequencies too large to appear as nulls in the spectra as they are drawn because of scale. The mixture of modes excited tends to favor low-frequency, high vertical wavenumber fluctuations for typical burst durations (5–10 d, lower two panels, Fig. 6). Wind patterns that grow and decay more gradually than the boxcar idealization used here will excite different mixtures of modes, but interference of the wave wakes from the leading and trailing edges of a wind event will like-

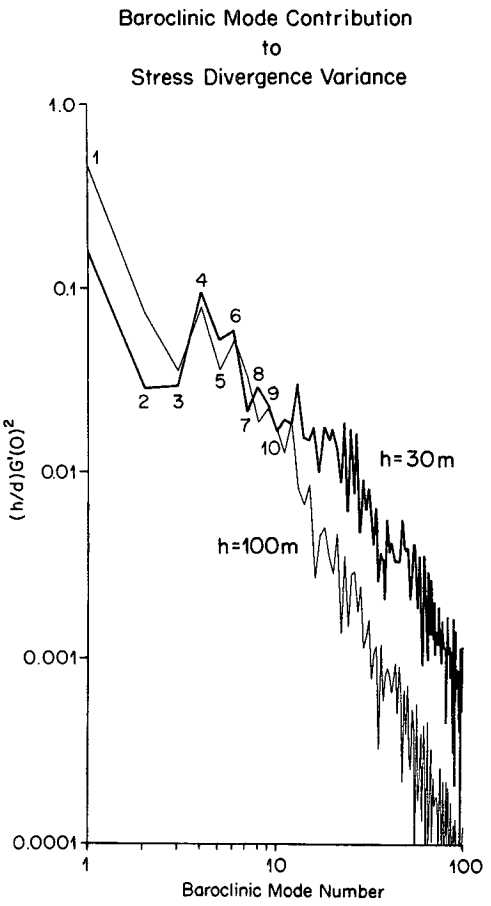

FIG. 3. Fractional contribution $(h/d)G'_m(0)^2$ of each baroclinic mode m to describing stress divergence variance (where stress divergence is uniform in a surface mixed layer of depth, h, and otherwise vanishes) based on the modal structures plotted in Fig. 2. Note $\Sigma_m(h/d)G'_m(0)^2) = 1$. The heavy (light) curve depicts contributions for $h = 30$ m ($h = 100$ m). Contributions at various modes m are labeled by number.

wise tend to produce spectral nulls at the fundamental frequency given by burst duration and its harmonics.

The spectral description given here identifies which wave modes are excited by a given wind, but phase information which describes how the modes sum together to produce current and pressure fields is suppressed. It is clear from the examples given here that a modal description, while convenient analytically, is not particularly efficient. When the modes are summed, however, the resulting flow fields are less complicated than the spectral description suggests at first glance.

4. Wave response flow fields

The flow fields found from summing a large number of modes appear as simple, smooth functions of location as long as sufficient numbers of modes are included in what formally are infinite sums [the solution given by (7), (11), and (12)]. The spectral description given above guides a sensible choice of the number of modes necessary to describe flow fields accurately. The choices listed at the end of section 2 can be seen from the spectra in Fig. 6 to be sufficient because they include all but a few percent of the variance in each field. The resulting flow fields are presented here in a sequence of two-dimensional plots: latitude versus time at fixed depths, depth versus time at a fixed latitude, and depth versus latitude at fixed times. In these plots, current is depicted as a vector stick and vertical displacement as a vector stick with fixed orientation. Two wind burst idealizations are presented as examples, one centered on the equator and the other centered at 3°S, both with a boxcar zonal stress jump of 0.1 Pa, duration of 5 d, eastward translation speed $U = 10$ m s^{-1}, and width $L = 3.6°$. The relatively simple response flow fields that result are easily interpreted as identifiable parts of the solution.

Response to wind bursts can be thought of as the sum of an equatorial wave wake and a Yoshida jet from the leading edge of the burst and equal and opposite responses from the trailing edge. The Yoshida jet response is most prominent in zonal current and pressure alone, grows linearly with distance behind the burst edges, and is both confined to and uniform within the mixed layer. It is given by the two nontrigonometric terms in (11a) and (12a). The remaining response both oscillates and propagates three dimensionally. The upper two panels of Fig. 7 depict horizontal surface current vectors as functions of latitude and time after a burst passed by a fixed location. The lower two panels depict horizontal current at 50-m depth (beneath the 30-m deep mixed layer). Because the burst propagates eastward, time after the burst passes is equivalent to distance behind the burst, as labeled in Fig. 7. Eastward current sticks are plotted upward to highlight the Yoshida jet solution.

When the burst is centered at the equator, surface currents (upper left panel, Fig. 7) grow eastward linearly in time along the equator over the 5-d interval between the onset of eastward winds and their cessation as the trailing edge of the burst passes by. At this time, growth of the eastward jet is arrested as the equal, opposite, but lagged Yoshida jets generated by the burst edges interfere exactly to leave a steady zonal jet. During the 5-d growth interval, off-equatorial surface currents tend to converge water toward the equator as well as accelerate it zonally. Surface currents poleward of 1° both oscillate and turn anticyclonically. These oscillations are the wave wake of the burst. The wake resembles none of the individual meridional modes. Instead, the oscillations resemble near-inertial internal gravity waves at each latitude, since the frequency of oscillation is everywhere slightly above the local inertial frequency. The oscillation frequency ranges from less

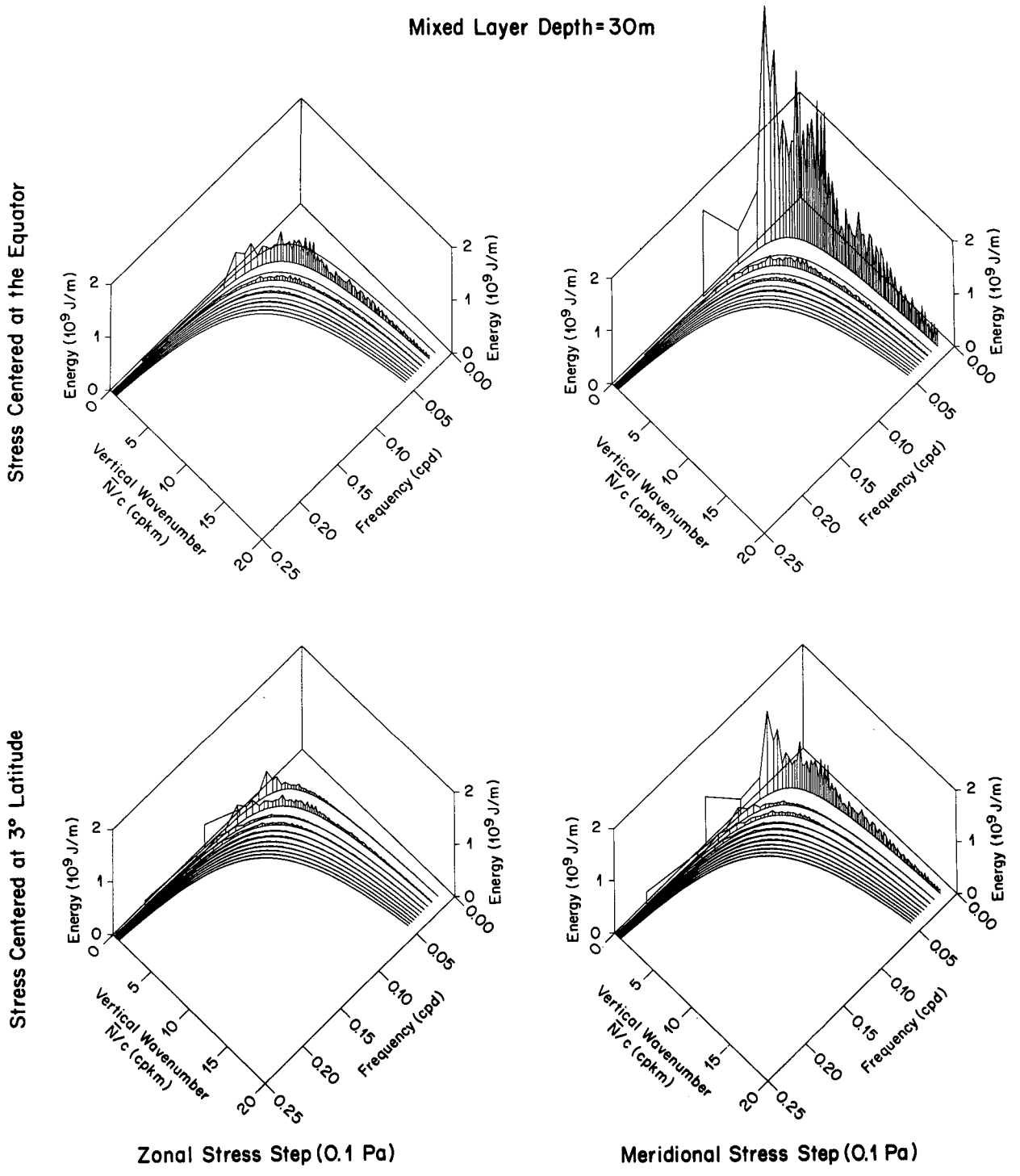

FIG. 4. Forced equatorial wave spectrum in response to a step function change in zonal (left panels) and meridional (right panels) wind stress of 0.1 Pa applied as a Gaussian with width $L = 3.6°$ in latitude centered on the equator (upper panels) and 3° latitude (lower panels), traveling eastward at $U = 10$ m s^{-1}. Plots are drawn for the first 100 baroclinic and zeroth (Rossby–gravity) through tenth (gravity) meridional modes. Spectrum is expressed as total wave energy (horizontal kinetic plus potential) in the equatorial waveguide per unit zonal distance. Estimates (vertical line segments) are connected at top and bottom to estimates at adjacent baroclinic modes for each meridional mode to illustrate the dispersion character of waves and for clarity. Equivalent vertical wavenumbers have been calculated as $\int_{-d}^{0} N(z)c_m^{-1}\,dz$. Calculations are based on the vertical modes for $h = 30$ m drawn in Fig. 2.

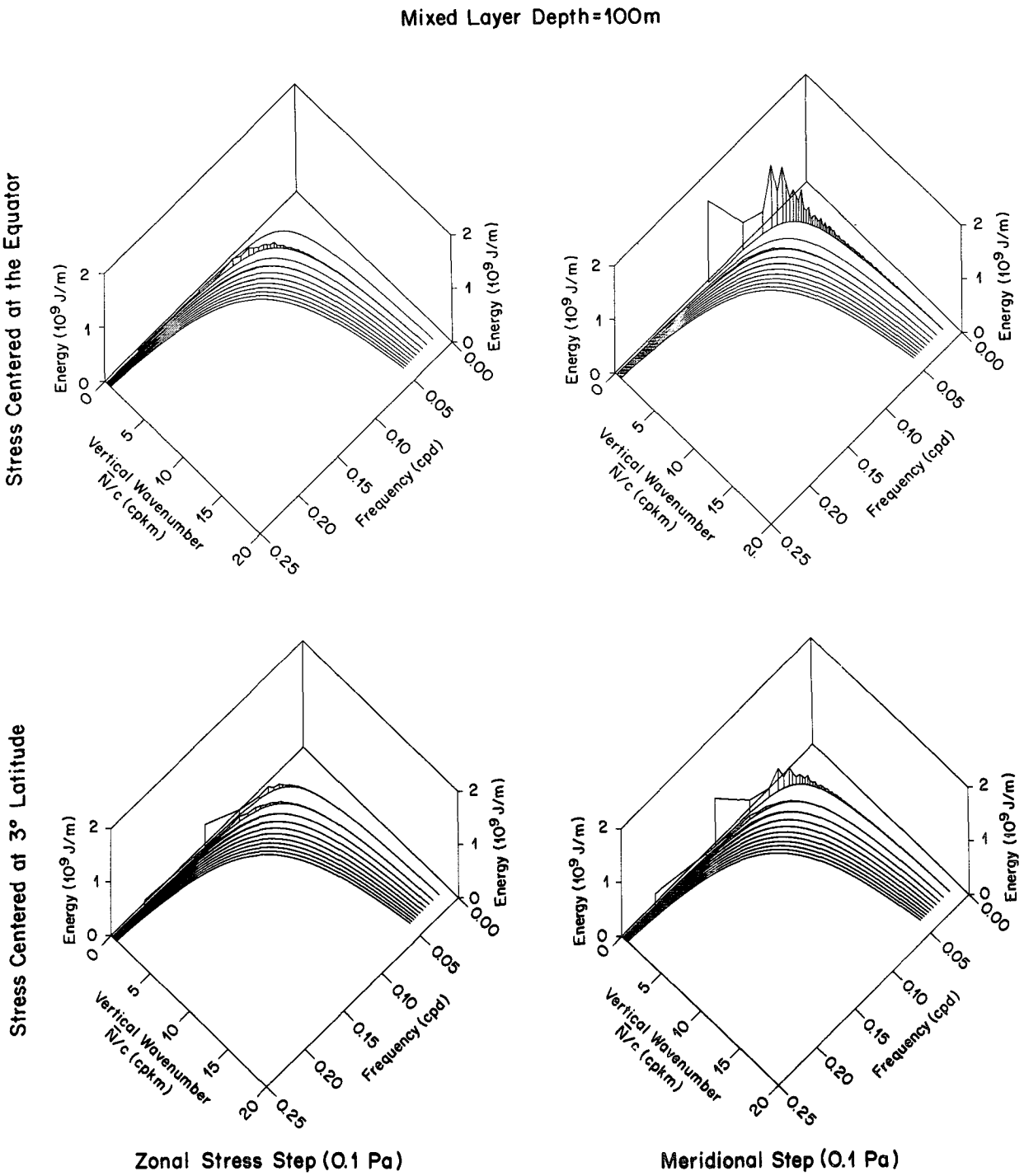

FIG. 5. Forced equatorial wave spectrum for mixed-layer depth h = 100 m plotted exactly as in Fig. 4.

than 1% above the local inertial frequency at 5° latitude to 55% above it at 1° latitude.

When the burst is centered off the equator at 3°S (upper right panel, Fig. 7), the Yoshida jet development still takes place, although more weakly, since winds in the vicinity of the equator are much weaker. Currents are prominent in the hemisphere where the wind patch occurs and also oscillate at what amounts to slightly superinertial frequency against a background of eastward flow.

The response at depth is made up entirely of wave response. Only slightly deeper than the mixed layer,

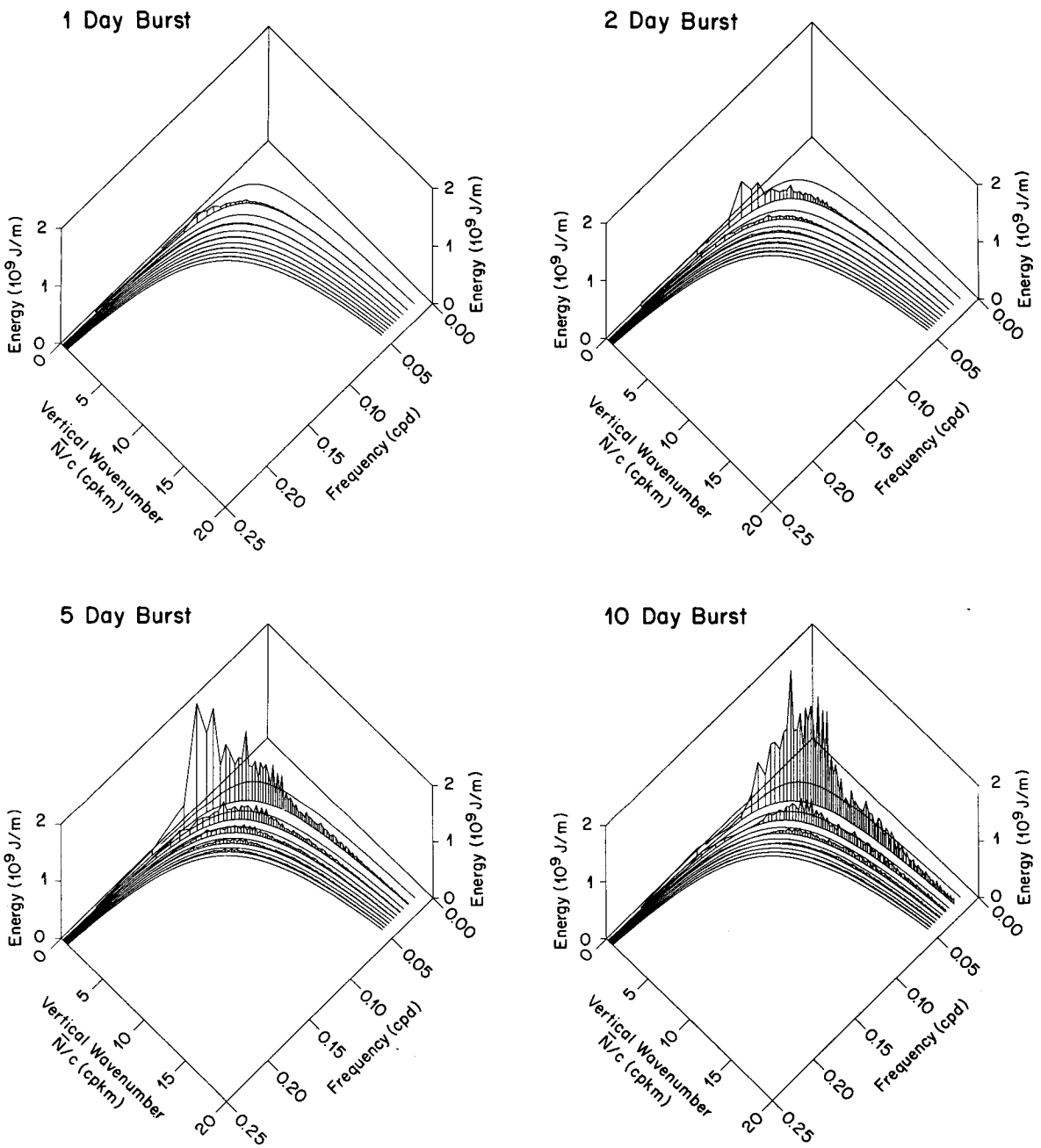

FIG. 6. Forced equatorial wave spectra in response to boxcar function changes of varying duration (as labeled by panel) in zonal wind stress of 0.1 Pa applied as a Gaussian with width 3.6° in latitude centered at 3° latitude where mixed-layer depth h = 30 m, plotted as in and with the same scales as the previous two figures.

currents tend to diverge water meridionally at the equator at the same time surface waters converge, and conversely, leading to a varicose oscillation along the equator (lower left panel, Fig. 7). The wave wake is concentrated initially at the latitude of forcing, but propagates, as will be discussed below.

The pressure field is expressed at the surface as sea level, and deeper as internal displacement. The upper panels of Fig. 8 show the sea level signal that accompanies surface current. The Yoshida jet requires a positive sea level displacement and downward pycnocline displacement to maintain it geostrophically after the burst passes, as is evident in this figure, both when the burst is centered on the equator and when it is centered south of it. The oscillatory character of the wave wake in sea level differs from that for current, though. For

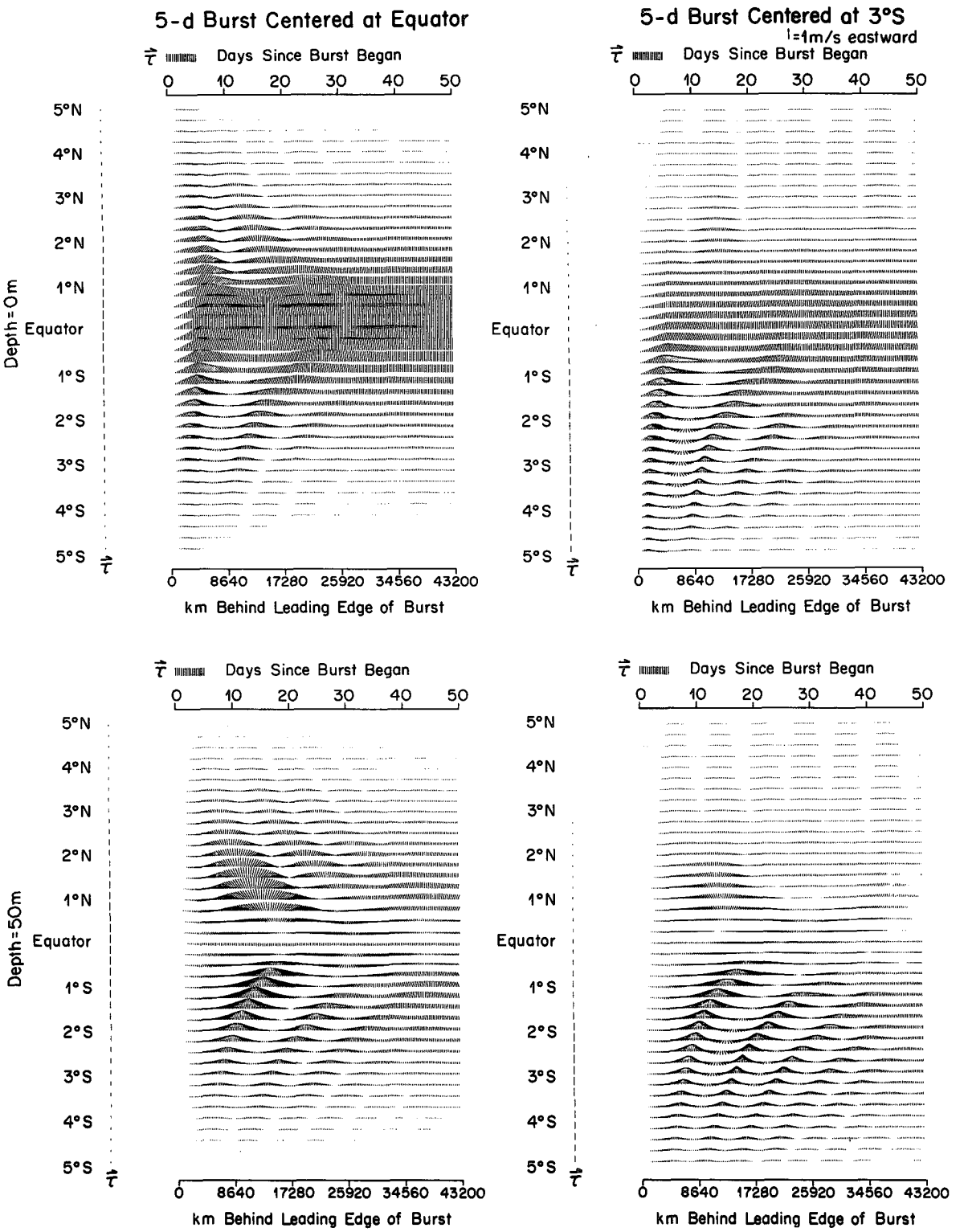

FIG. 7. Horizontal currents excited in response to bursts of westerly wind stress 5 d in duration centered at the equator (left panels) and at 3°S (right panels). Bursts travel eastward at speed $U = 10$ m s^{-1} and response is based on $h = 30$ m for the stratification described in Fig. 2. Upper (lower) panels depict currents at the surface (at 50-m depth). Currents are drawn as vector sticks every 8 h in time (288 km zonally) and every 0.25° in latitude. The current scale is given above the upper right panel: a vector stick equivalent in length to the separation between two time series and directed upward indicates eastward flow at 1 m s^{-1}. The temporal and meridional variation of stress is likewise indicated by vector sticks appearing alongside the plot axes (maximum stress is 0.1 Pa).

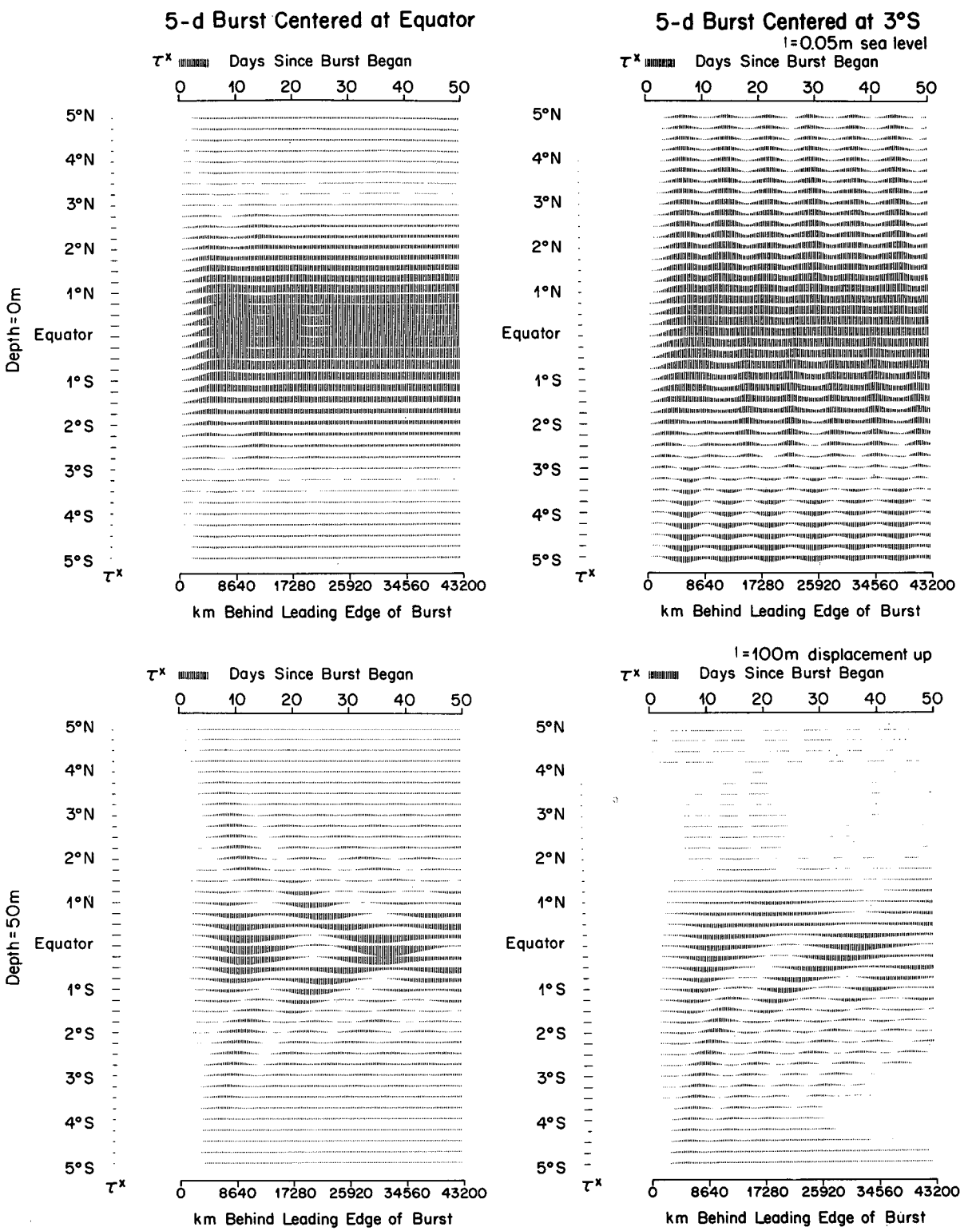

FIG. 8. Sea level (upper panels) and vertical displacement at 50-m depth (lower panels) for the same bursts and plotted similarly as in Fig. 7. A stick directed upward and equal in length to the separation between two time series indicates upward displacement of sea level and isopycnals by 0.05 and 100 m, respectively.

both forcings depicted in Fig. 8, sea level oscillations are not at all centered near the local inertial frequency. Rather, sea level resembles one or two grave meridional modes beating against one another at periods of 4–5 d. This appearance, despite the vigorous excitation of higher modes in the solution, is because a sea level signal filters out contributions from higher baroclinic modes quite effectively (Wunsch and Gill 1976). However, the internal displacement signal (lower panel) has a character very similar to current in that oscillation frequencies are locally somewhat superinertial. Unlike midlatitude near-inertial internal gravity waves, equatorial gravity waves generate substantial internal displacements even at locally near-inertial periods due to the relatively high gradient of planetary vorticity compared to planetary vorticity itself.

Remarkably, predicted currents and vertical displacements for a modest 0.1-Pa wind burst strength are rather large. For example, horizontal currents vary by as much as 1 m s^{-1} between the bottom of the mixed layer and 50-m depth and between the equator and 1° latitude (left panels, Fig. 7). Similarly, downward displacements of as much as 100 m are predicted for isopycnals found at 50-m depth at rest (lower left panel, Fig. 8). These excessive shears and strains are well above what is ever observed in the open ocean. Clearly, the linear prediction will fail to satisfy fully nonlinear equations of motion for amplitudes as high as these. Discussion of the range of validity of the linear solution is deferred to the next section. The linear results presented here can be regarded as valid for suitably weak wind stress forcing.

The wave wake of a wind burst, while formally constructed from vertically standing modes, appears as a downward-directed beam of equatorial waves in the upper ocean. Current fluctuations beneath the mixed layer display the upward phase propagation characteristic of a downward-directed beam (Fig. 9). The current vector also turns anticyclonically with depth, just as with midlatitude near-inertial internal gravity waves sending energy downward. The locally near-inertial oscillation of currents appears to be superposed upon a "mean" zonal current directed in the same direction as flow in the mixed layer. The source of this very low-frequency current well beneath the mixed-layer jet is not clear.

While the assumption of a large translation speed U leads to the generation of waves with very long zonal scale (see Fig. 1), meridional scales are much shorter. Meridional currents of short meridional scale drive convergence variations that produce vertical current fluctuations. Examples of motions in the vertical–meridional plane are given in Fig. 10, where the scale vector applies only to the meridional component of the vector sticks drawn. The vertical component of current has been exaggerated identically to the exaggeration of the vertical axis so that the slopes of the stick vectors drawn represent the direction of flow in

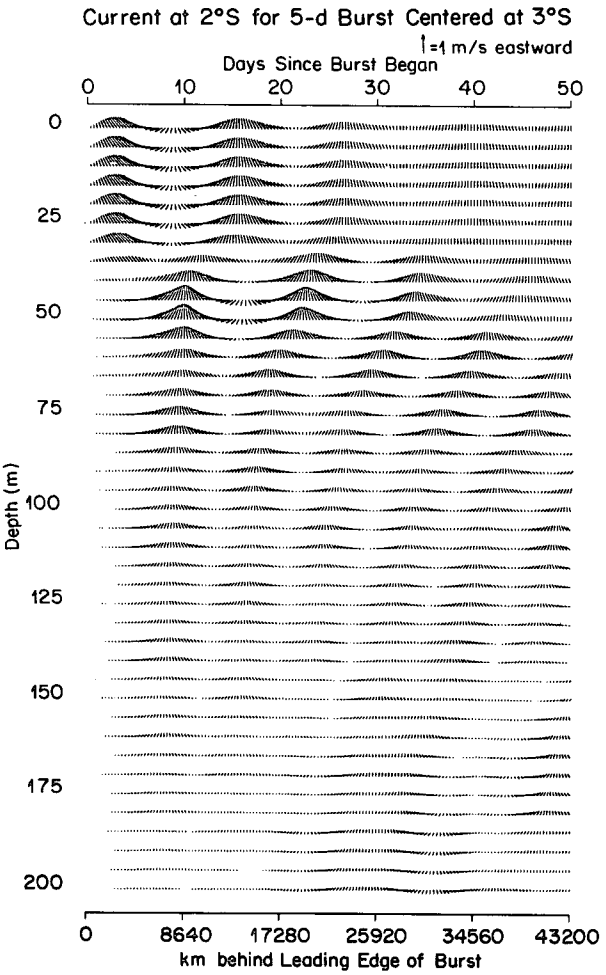

FIG. 9. Horizontal currents in the upper 200 m at 2°S excited in response to the same westerly burst as in the right panels of Figs. 7 and 8. Currents are plotted as stick vectors as in the panels of Fig. 7 and to the same scale except that they are plotted against depth instead of against latitude.

reference to the axes. The panels of Fig. 10 show the development of a series of vertical–meridional cells with increasing time after the passage of a burst. One broad cell is centered initially at the latitude of forcing and has its highest amplitude near the base of the mixed layer (30 m). The cell moves equatorward in time as others form behind it and also migrate equatorward. For the case shown, where the wind burst was centered at 3°S, the beam of equatorial waves shifts northward as it penetrates more deeply. This pattern can be interpreted as the refraction of rays on the equatorial β plane. These rays cross into the other hemisphere and can be expected to turn back equatorward when the local inertial frequency grows to match the wave frequency.

Meridional structure develops in the solution as a consequence of the spatial variation of the inertial frequency $f = \beta y$. Because the wave wake is dominated

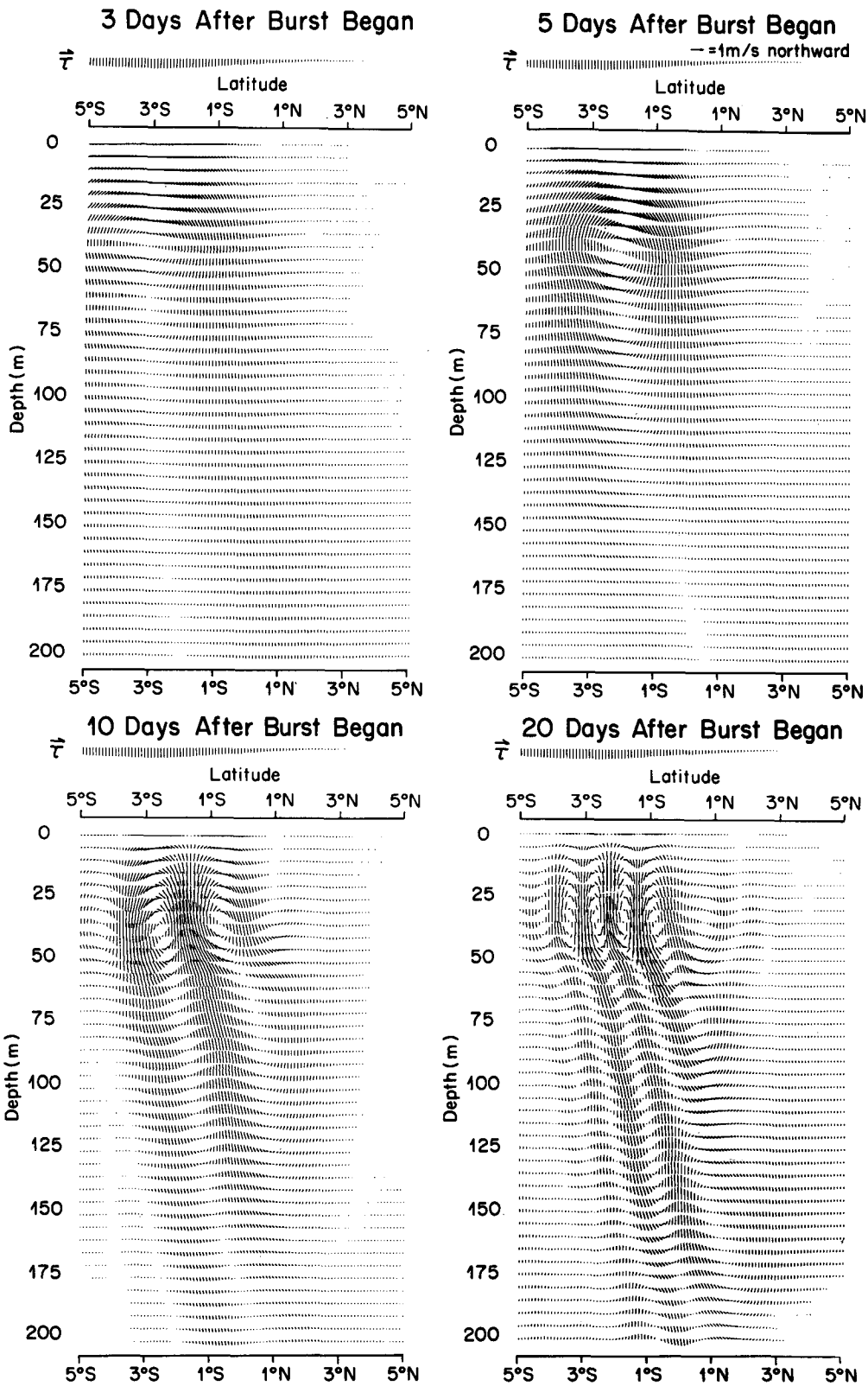

FIG. 10. Currents in the vertical–meridional plane excited by the same westerly wind burst as in Fig. 9 and the right panels of Figs. 7 and 8 plotted for various times after the start of the 5-d burst. Currents are plotted as stick vectors where the scale in the upper right panel applies only to the meridional component (a stick equal in length to the 5-m depth separation depicted and directed to the right indicates northward current of 1 m s^{-1}). The vertical component of current is exaggerated identically to the vertical exaggeration of the depth axis relative to the latitude axis so that vector sticks preserve slope of currents rather than current magnitude.

by locally near-inertial oscillations, oscillations at neighboring latitudes develop phase differences in only a few days, as is apparent in Figs. 7 and 10. The meridional scale of the wave wake decreases roughly as $(\beta t)^{-1}$ after the passage of a burst, just as with near-inertial waves generated by a storm at midlatitudes (D'Asaro 1989). The steady decrease of meridional scale as the wake disperses leads directly to the failure of the linear solution to satisfy fully nonlinear equations of motion. This breakdown is considered next.

5. Advection implied by the linear solution

The linear solution described here is only valid when the linear system (1) is a valid approximation to the full equations describing momentum and thermodynamic energy conservation. The validity of the linear solution can be verified by calculating advection of momentum and density from this solution and comparing these terms to the linear terms in these equations. Using the linear solution to estimate nonlinear terms serves to identify the locations where the linear conservation equations (1) do not apply for a given wind stress strength and structure. This procedure extends what can be found from scale analysis by demonstrating both which advection terms break the assumption of linear dynamics and where in the flow the breakdown occurs.

The linear system (1) is based on simplification of the full equation for thermodynamic energy conservation to one for density. In the absence of mixing, density conservation is expressed as:

$$\rho'_t + u\rho'_x + v\rho'_y + w(\rho_{1z} + \rho'_z) = 0, \qquad (17)$$

where $\rho(x, y, z, t) \equiv \rho_0 + \rho_1(z) + \rho'(x, y, z, t)$. Through the hydrostatic equation $p_z = -g\rho'/\rho_0$, density conservation (17) may be expressed as

$$Up_{zx} - up_{zx} - vp_{zy} - N^2 w - wp_{zz} = 0, \qquad (18)$$

where u, v, p, and w are the nonlinear flow field variables. Substituting the linear quantities identified in the decomposition (2), the estimates of the size of terms in (18) can be found easily by differentiating (12) analytically. Since $U \gg u$, the second term in (18) can be neglected. Estimates of the remaining terms are plotted in Fig. 11 for the case of 3 d after the start of a 5-d long, 0.1-Pa zonal burst centered at 3°S. The two nonlinear advection terms $v\rho'_y$ and $w\rho'_z$ are minuscule compared to the basic linear balance of local rate of change with vertical advection of the basic stratification. Nonlinear advection becomes large at later stages according to the linear estimate, but linear momentum conservation has already broken down only 3 d after the burst began, as will be shown next.

While scaling arguments demonstrate that vertical momentum conservation is hydrostatic for time scales short compared to N^{-1}, advection of momentum can alter the balance of horizontal momentum from (1a,b) to

$$u_t + uu_x + vu_y + wu_z - fv = -p_x + \tau^x/h \qquad (19a)$$

$$v_t + uv_x + vv_y + wv_z + fu = -p_y + \tau^y/h. \qquad (19b)$$

The linear inviscid terms in (19) are plotted as vectors in Fig. 12 for the same forcing as in Fig. 11 along with $\mathbf{u}\cdot\nabla\mathbf{u}$, the total advection of horizontal momentum (lower left panel), estimated from the linear solution (7), (11), and (12) and its appropriate derivatives. The horizontal momentum balance is effectively linear deeper than about 100-m depth at this point during the burst (3 d after its start), but linear estimates of the nonlinear terms are comparable to the linear terms in the balance at shallower depths directly beneath the wind burst. Scaling shows that zonal advection cannot be important but that advection in the meridional plane can be. Estimation with the linear solution of the second two terms in (19) as scalars (Fig. 13) shows that meridional and vertical advection are the sources of nonlinearity in the mixed layer and upper pycnocline, respectively, at this stage of burst response.

These calculations call the validity of the linear solution into serious question for wind bursts of the size observed in the western Pacific applied to mixed layers of typical preburst size. However, when the same burst as in Figs. 11–13 has stress applied through a deeper mixed layer (100 m instead of 30 m), a linear momentum balance is much more valid, even 5 d after the burst began (Fig. 14). In this case, horizontal advection in the mixed layer is negligible and vertical advection appears at most mildly important only in a thin region at the top of the pycnocline. Applying stress through a thicker mixed layer delays the development of nonlinearities because currents are weaker (compare top panels in Fig. 14 with those in Fig. 12); hence development of significant advection in the vertical–meridional plane.

6. Mixing suggested by the linear solution

The linear system (1) neglects more than advection, it also neglects turbulent diffusion of momentum (outside the mixed layer of prescribed constant thickness) and of mass. The real ocean does mix, particularly the upper ocean, so it is worth examining whether the linear solution predicts conditions favorable for mixing. While parameterizations for mixing in stratified fluids are imperfectly known, it is well recognized that vigorous mixing takes place when the gradient Richardson number $\mathrm{Ri} \equiv -g\rho_z\rho_0^{-1}/(u_z^2 + v_z^2)$ is reduced somewhat below unity (Gregg 1987). The linear solution predicts a density gradient $\rho_z = \rho_{1z} + \rho'_z = -\rho_0(N^2 + p_{zz})/g$ giving a linear estimate of $\mathrm{Ri} = (N^2 + p_{zz})/(u_z^2 + v_z^2)$. As mentioned previously, reasonable choices for wind burst strength lead to rather large estimates of vertical shear by the linear model. They also lead to

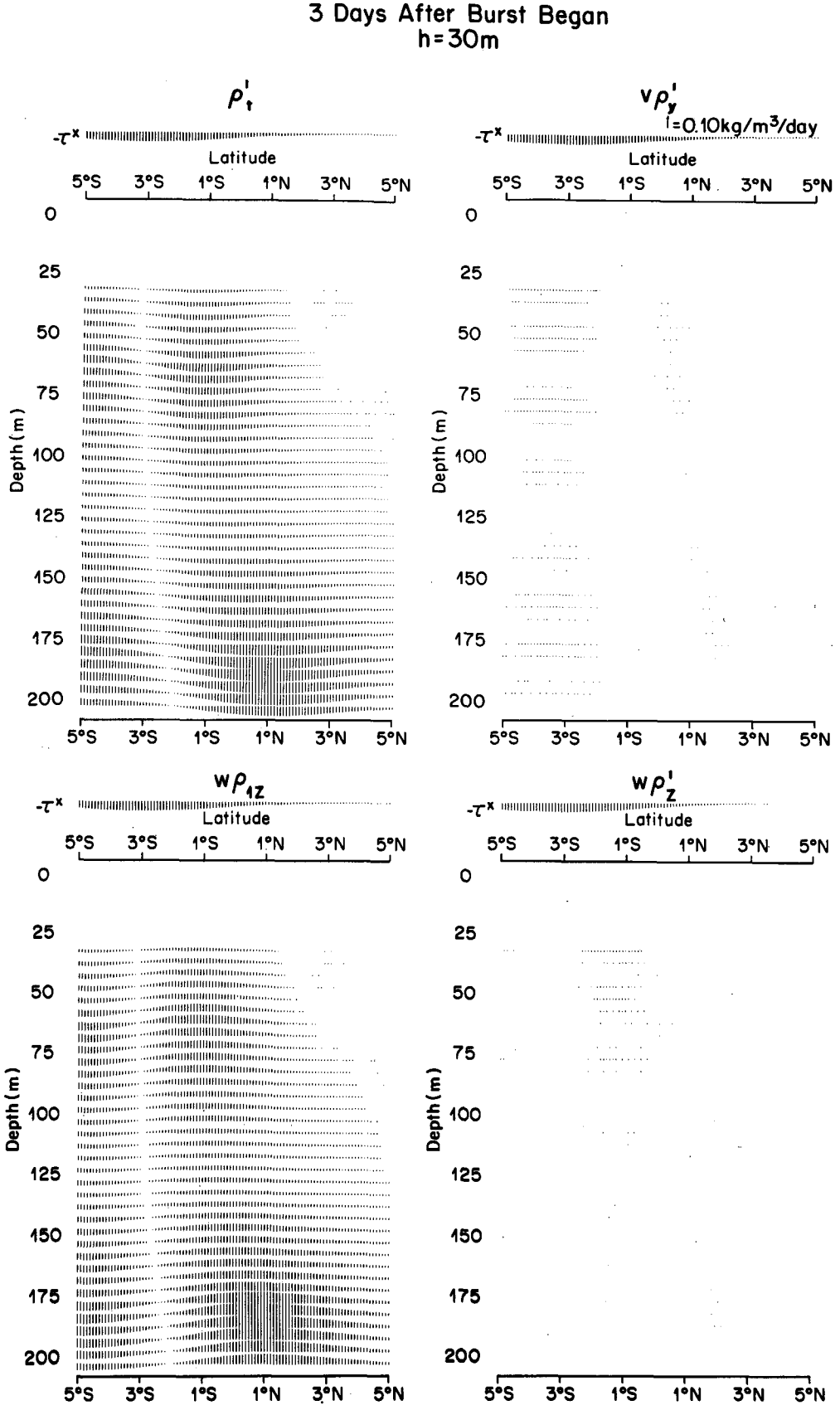

FIG. 11. Terms of the density balance in the vertical–meridional plane 3 d after the start of the same 5-d burst as in Fig. 9. Left panels depict the linear balance between local rate of change of perturbation density ρ'_t and vertical advection of the background stratification $w\rho_{1z}(z)$. Right panels depict linear estimates of meridional and vertical advection of perturbation density.

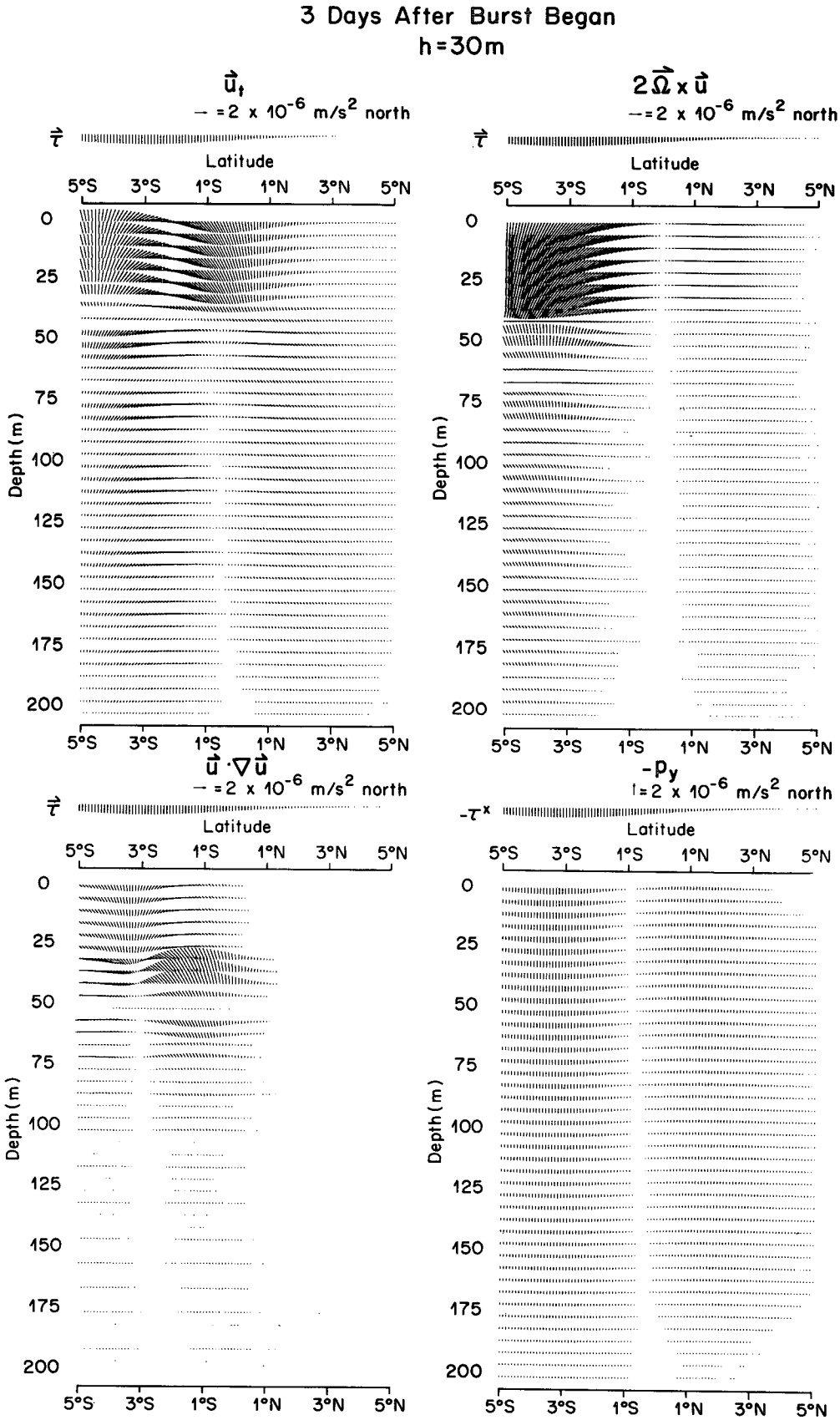

FIG. 12. Terms of the horizontal momentum balance evaluated in the vertical–meridional plane 3 d after the start of the same 5-d burst as in Figs. 9 and 10. Local acceleration (upper left panel), Coriolis acceleration (upper right panel), and a linear estimate of momentum advection (lower left panel) are plotted as vector sticks (eastward component down, northward component to the right, where a stick the same length as the 5-m depth separation corresponds to acceleration of 2×10^{-6} m s^{-2}). The meridional component of pressure gradient force per unit mass is plotted to the same scale, but with north up for clarity (lower right panel).

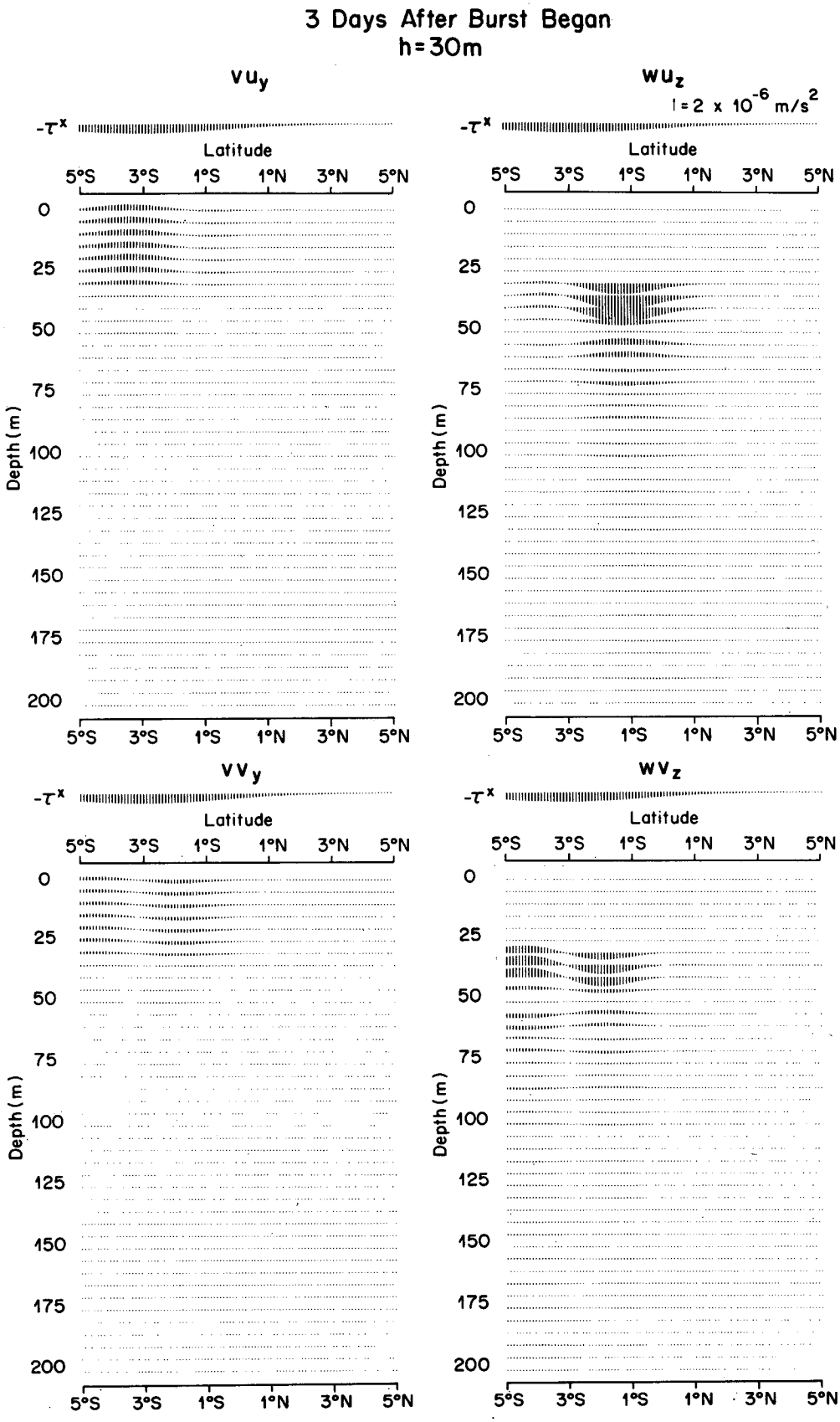

FIG. 13. Principal advection components of the horizontal momentum balance for the same burst as in Fig. 12. These terms are plotted as in Fig. 12 as scalars instead of vectors, where positive quantities are upward.

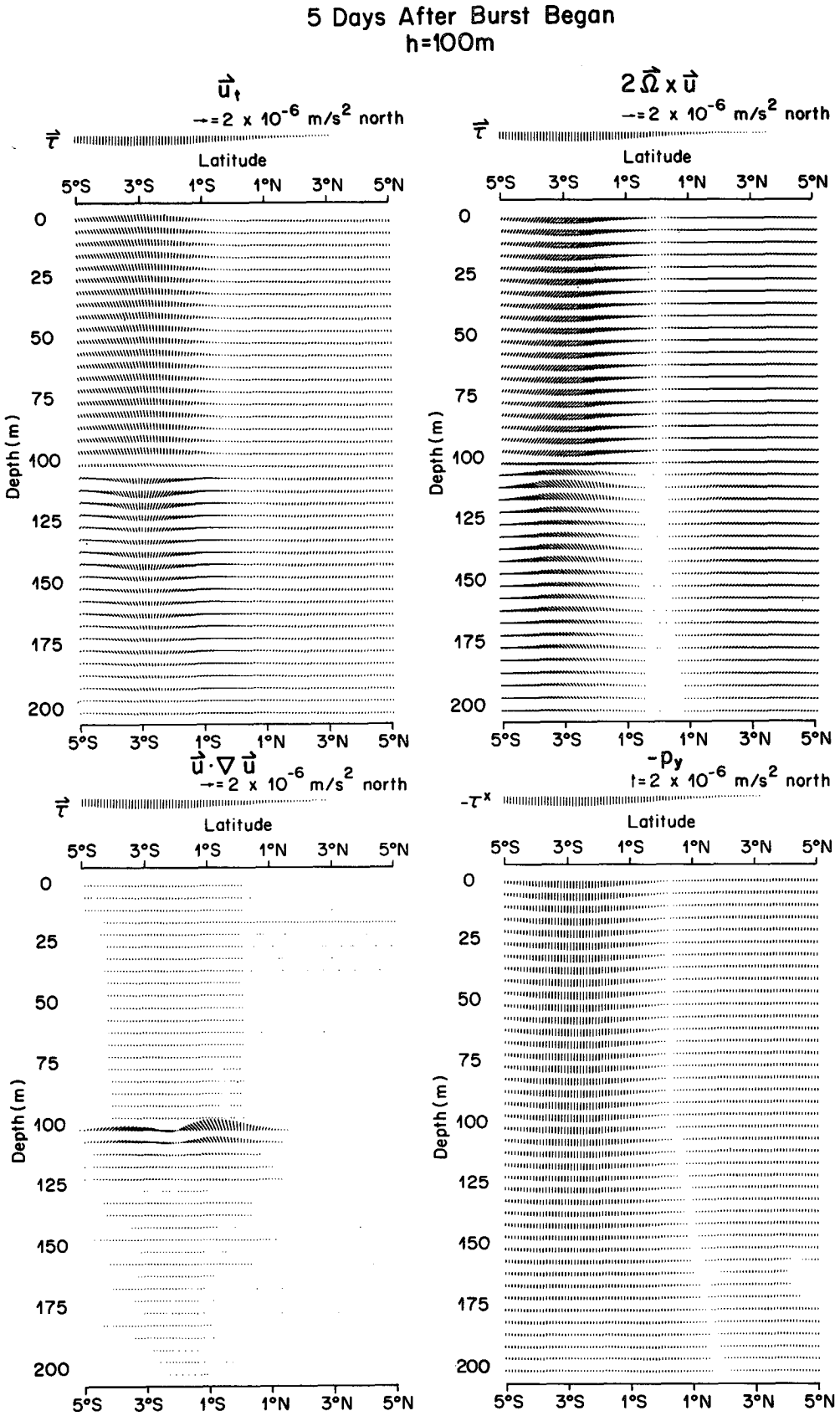

FIG. 14. Terms of the horizontal momentum balance evaluated in the vertical–meridional plane 5 d after the start of a burst identical to the one considered in Figs. 9–13, except for a mixed-layer depth h of 100 m, plotted as in and to the same scale as Fig. 12.

large values for the local buoyancy frequency, but not large enough for the local Richardson number to remain above unity.

Using the burst examples cited in the previous section, estimates of shear magnitude (left panels), and a vector whose upward component is shear magnitude squared and rightward component is local buoyancy frequency squared (right panels) are plotted in Fig. 15. The slope of the vector sticks above the horizontal axis is Ri^{-1}. Shear in both cases is concentrated at the base of the mixed layer and Ri is locally reduced well below unity in both cases. Local Ri remains much greater than unity within the deeper portion of the thermocline portrayed (i.e., depth 150 m and deeper). The size of the shear is sensitive to the number of vertical modes used in the solution; to faithfully depict the velocity transition between a fixed mixed layer over which stress is applied and a frictionless pycnocline beneath it requires an infinite number of modes. The local Ri predicted is well less than unity for any sum of modes truncated reasonably. While the 100-m deep mixed-layer case is less extreme, both cases in Fig. 15 suggest conditions for which mixing will occur. Significantly, conditions become favorable for mixing well before the development of nonlinearities according to the linear solution.

7. Discussion and conclusions

The purpose of developing this model was to provide guidance in what equatorial wave response to expect for an actual westerly wind burst in the western Pacific Ocean. Although the model is reasonably realistic with respect to characterizing the wind bursts as meridionally confined, rapidly eastward-propagating disturbances, there are aspects for which the model is unrealistic. The model was also developed because numerical simulations have generally ignored or suppressed equatorial gravity wave response to westerly bursts. Although the linear model presented here is an exercise in geophysical fluid dynamics rather than a simulation, it demonstrates that gravity wave response may dominate current and internal displacement fields in the upper ocean. Because the wave response includes development of energetic shear and strain variability, it is crucial in determining how stratification will evolve through mixing. Since it extends beyond the Yoshida jet, in both meridional extent and in depth, wave response is particularly important to generating mixing over broad regions of the tropical ocean. At the very least, pycnocline distortions due to waves must be distinguished from those due to mixing for field measurements to be interpreted properly. This task is particularly difficult at low latitudes because the wave wake behind a wind burst generates substantial vertical strain from convergence of horizontal currents. In contrast, storm-generated near-inertial internal gravity waves at midlatitude include only fairly small internal displacements.

The calculations presented here apply to a laterally boundless, resting equatorial β-plane ocean with a flat bottom. The real western Pacific has a circulation and is rich in islands and undersea topography. Since all the waves in the linear solution have phase speeds equal to the wind burst translation speed and this speed is much faster than any current, the wave wake is not expected to interact significantly with the mean circulation. Because response is confined reasonably to the latitudes of forcing and wind bursts are relatively localized, the equatorial β-plane wave modes can be expected to imitate those of a spherical or spheroidal earth fairly well. Because wave response is concentrated in the upper ocean and travels vertically relatively slowly, neglect of deep-bottom topography is also reasonable. However, shallow bottom topography, particularly island coasts, can be expected to influence response only within the latitude range that wind burst forcing is applied. In the western Pacific, relevant boundaries are relatively close zonally; the distance from the Celebes to the Gilbert Island Group is only 5000 km or so. The zonal proximity of boundaries can be expected to alter the character of the wave wake, comprised as it is of waves with O(10 000 km) wavelengths. Proximity to boundaries does not prevent equatorial gravity waves from being generated altogether, since at least low baroclinic modes of these waves with comparably long zonal wavelengths account for observed spectral peaks in island sea level records (Wunsch and Gill 1976; Luther 1980).

Westerly wind bursts in this model have been assumed to translate without change of form or intensity. By contrast, other models of these bursts take them to grow and decay in place as stationary features (e.g., Giese and Harrison 1990, 1991). Presumably, actual wind burst events develop with a mixture of both propagating and evolving characteristics. Bursts are observed to develop over the Indonesian archipelago and die away in the vicinity of the international date line (Nakazawa 1988). Nevertheless, they translate zonally at a brisk and roughly uniform rate. Equatorial gravity waves are generated because wind stress changes abruptly at a given location. The waves excited are comparatively long because the abrupt transitions in stress translate rapidly to the east in the vicinity of the equator. The idealized form for the wind taken here was chosen to replicate the crucial characteristics of westerly wind bursts while remaining simple enough that linear equations of motion could be solved analytically. Actual wind bursts can be expected to generate somewhat different wave wakes, but the result that the wave wake will be dominated by relatively high vertical mode equatorial gravity and Rossby–gravity modes will remain.

The estimates of nonlinear terms presented in section 5 indicate that, according to the model, wave response will cease to be linear only a few days after a burst of modest stress amplitude has begun. However, estimates of shear and Richardson number indicate that mixing

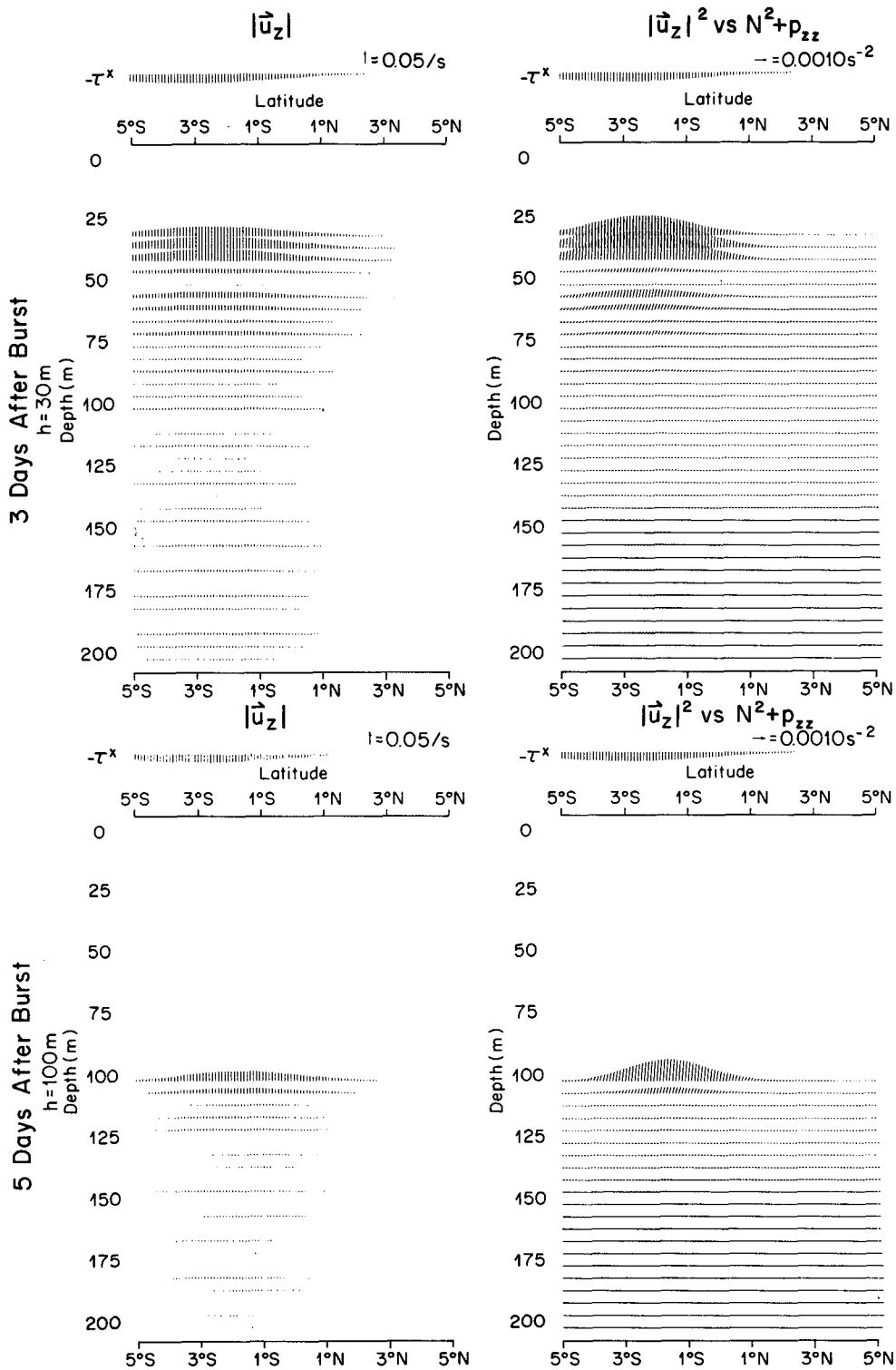

FIG. 15. Magnitude of vertical shear of horizontal current (left panels) and a vector whose components are shear squared and background plus perturbation buoyancy frequency squared (right panels) at a time 3 d (upper panels) and 5 d (lower panels) after the start of the same burst as in Figs. 9–14 for h = 30 m (upper panels) and h = 100 m (lower panels). Sticks equal in length to the 5-m depth separation correspond to 0.05 s^{-1} in shear and 0.001 s^{-1} in square shear (upward) and $N^2(z) + p_{zz}$ (to the right).

of mass and momentum will become vigorous in the upper pycnocline within a day after the start of a burst. The model is unrealistic in that mass mixing is precluded and momentum mixing is confined to a mixed layer of constant prescribed depth. Wave response is expected to be weaker in the ocean than in the model both because wind stress is spread over an ever-thickening mixed layer and because wave energy is lost to mixing the upper pycnocline. Together these processes can be expected to delay the development of nonlinear wave momentum balances or prevent them altogether. Observations of upper-ocean turbulent dissipation rates in the western Pacific (M. Gregg and K. Brainerd 1991, personal communication) indicate that mixing is sufficiently intense in a wind burst to absorb the kinetic energy of a wave wake on time scales of several days. Unfortunately, the modal decomposition employed here works only for separable vertical and horizontal forcing structure. A more realistic model would employ numerical techniques to simulate the temporal structure of wind stress convergence within an actively deepening mixed layer. The response can be expected to remain reasonably linear for even strong wind burst forcing as long as the mixed layer deepens sufficiently and wave energy is siphoned into potential energy increase.

Westerly wind burst forcing is a plausible candidate for generation of spectral peaks in island sea level. Luther (1980) noted that variance in given peaks varies seasonally and interannually. The occurrence of westerly wind bursts also has significant variation on these time scales. The Wunsch and Gill explanation of peaks in sea level spectra is that broadband wind forcing leads to wave energy accumulating at nulls in zonal group speed for low baroclinic-mode equatorial gravity waves. These frequencies are indistinguishable in most observations from frequencies for which zonal wavenumber vanishes (Luther 1980; Eriksen 1982). They are also indistinguishable from frequencies corresponding to waves forced with high phase speeds, that is, speeds comparable to translation speeds of westerly bursts. Wunsch and Gill (1976) and Luther (1980) demonstrated coherence between local meridional wind and island sea level, identifying it as the source. Luther (1980) also noticed that observed sea level peaks tended to occur at frequencies a few percent higher than those predicted for waves of vanishing zonal group speed. The model presented here indicates that translating wind bursts can be potent generators of spectral peaks in sea level at frequencies several percent higher than the minimum for low meridional-mode equatorial gravity waves and that bursts of zonal as well as of meridional stress are possible sources of sea level oscillations.

Acknowledgments. This work was motivated by and benefited from planning discussions of the Science Working Group for the Tropical Oceans–Global Atmosphere Coupled Ocean Atmosphere Response Experiment (TOGA-COARE). R. Lukas provided western Pacific CTD casts that were used to form average buoyancy frequency profiles from which baroclinic modes were calculated. D. Moore showed the author how to evaluate the integral of the product of a Gaussian and a Hermite function. I thank the officers and crew of the NOAA Ship Baldrige for the opportunity to make extensive equatorial computations while steaming 4444 km along the equator. This work was supported by National Science Foundation Grant OCE-8811172.

REFERENCES

D'Asaro, E. A., 1989: The decay of wind-force mixed layer inertial oscillations due to the β effect. *J. Geophys. Res.*, **94,** 2045–2056.

Drake, Sir Francis, 1628: The World Encompassed. *The World Encompassed and Analogous Contemporary Documents Concerning Sir Francis Drake's Circumnavigation of the World.* N. M. Penzer, Ed., Cooper Square Publishers, 1969, 235 pp.

Eriksen, C. C., 1982: Equatorial wave vertical modes observed in a western Pacific island array. *J. Phys. Oceanogr.*, **11,** 1206–1227.

Giese, B. S., and D. E. Harrison, 1990: Aspects of Kelvin wave response to episodic wind forcing. *J. Geophys. Res.*, **95,** 7289–7312.

——, and ——, 1991: Eastern equatorial Pacific response to three composite westerly wind types. *J. Geophys. Res.*, **96,** 3239–3248.

Gregg, M. C., 1987: Diapycnal mixing in the thermocline: A review. *J. Geophys. Res.*, **92,** 5249–5286.

Harrison, D. E., and B. S. Giese, 1991: Episodes of surface westerly winds as observed from islands in the western tropical Pacific. *J. Geophys. Res.*, **96,** 3221–3237.

Kundu, P. K., and R. E. Thompson, 1985: Inertial oscillations due to a moving front. *J. Phys. Oceanogr.*, **15,** 544–565.

Lessa, W. A., 1984: Drake in the South Seas. *Sir Francis Drake and the Famous Voyage, 1577–1580.* N. J. W. Thrower, Ed., University of California Press, 60–77.

Lighthill, M. J., 1969: Dynamic response of the Indian Ocean to the onset of the southwest monsoon. *Philos. Trans. Roy. Soc. London, A,* **265,** 45–92.

Lukas, R., and E. Lindstrom, 1991: The mixed layer of the western equatorial Pacific Ocean. *J. Geophys. Res.*, **96,** 3343–3357.

Luther, D. S., 1980: Observations of long period waves in the tropical oceans and atmosphere. Ph.D. thesis, MIT-WHOI Joint Program in Oceanography, Woods Hole Oceanographic Institution Tech. Rep. WHOI-80-17, 210 pp.

——, D. E. Harrison, and R. Knox, 1983: Zonal winds in the central equatorial Pacific and the onset of El Niño. *Science,* **222,** 327–330.

McCreary, J. P., Jr., 1980: Modelling wind-driven ocean circulation. Hawaii Institute of Geophysics Tech. Rep. HIG-80-3, 64 pp.

——, and R. Lukas, 1986: The response of the equatorial ocean to a moving wind field. *J. Geophys. Res.*, **91,** 11 691–11 705.

Moore, D. W., and S. G. H. Philander, 1978: Modelling of the tropical ocean circulation. *The Sea,* Vol. 6, Interscience 319–361.

Nakazawa, T., 1988: Tropical super clusters within intraseasonal variations over the western Pacific. *J. Meteorol. Soc. Japan,* **66,** 823–839.

Quinn, W. H., V. T. Neal, and S. E. Antunez de Mayolo, 1987: El Niño occurrences over the past four and a half centuries. *J. Geophys. Res.*, **92,** 14 449–14 461.

Sugden, J., 1990: *Sir Francis Drake.* Henry Holt, 353 pp.

Wilson, D., 1977: *The World Encompassed: Drake's Great Voyage 1577–1580.* Hamish Hamilton, 240 pp.

Wunsch, C., and A. E. Gill, 1976: Observations of equatorially trapped waves in Pacific sea level variations. *Deep-Sea Res.*, **23,** 371–390.